

EKATERINA VAGAPOVA

Fluorescence quenching
in inorganic crystalline solids activated
by neodymium ions; from bulk
to micro- and nanocrystals



EKATERINA VAGAPOVA

Fluorescence quenching
in inorganic crystalline solids activated
by neodymium ions; from bulk
to micro- and nanocrystals



UNIVERSITY OF TARTU
Press

The study was carried out in the Institute of Physics, Faculty of Science and Technology, University of Tartu

The Dissertation was admitted on June 18, 2021, in partial fulfilment of the requirements for the degree of Doctor of Philosophy in Material Science and allowed for defense by Scientific Council on Material Science of the Faculty of Science and Technology, University of Tartu.

Supervisors: Dr. hab. Yury Orlovskiy
Institute of Physics, University of Tartu, Estonia

PhD Valter Kiisk
Institute of Physics, University of Tartu, Estonia

PhD. Viktor Peet, Institute of Physics, University of Tartu
Institute of Physics, University of Tartu, Estonia

Opponents: PhD Sergey Sekatskii
École Polytechnique Fédérale de Lausanne, Switzerland

Prof. Toomas Rõõm
National Institute of Chemical Physics and Biophysics,
Tallinn, Estonia

Defense: August 27, 2021, at University of Tartu, Estonia

This work has been supported by Estonian Research Council grant PRG347. This work has been partially supported by Graduate School of Functional materials and technologies receiving funding from the European Regional Development Fund in University of Tartu, Estonia.



European Union
European Regional
Development Fund



Investing
in your future

ISSN 2228-0928

ISBN 978-9949-03-669-1 (print)

ISBN 978-9949-03-670-7 (pdf)

Copyright: Ekaterina Vagapova, 2021

University of Tartu Press
www.tyk.ee

CONTENTS

LIST OF PUBLICATIONS INCLUDED IN THE THESIS	7
Other publications	7
1. INTRODUCTION	8
2. RESEARCH TASK	11
3. STATEMENTS PRESENTED FOR THE DEFENCE	12
4. EXPERIMENTAL	13
4.1. Synthesis of the materials	13
4.1.1. Synthesis of the Nd^{3+} : LaF_3 bulk crystals	13
4.1.2. Synthesis of the colloidal solutions of Nd^{3+} : LaF_3 and Nd^{3+} : KY_3F_{10} nanoparticles	13
4.1.3. Synthesis of the Nd^{3+} : $\text{Ca}_3(\text{PO}_4)_2$ microceramics.....	14
4.2. Measurement technique	15
4.2.1. Energy-dispersive X-ray spectroscopy	15
4.2.2. X-Ray diffraction analysis	15
4.2.3 Transmission electron microscopy	15
4.2.4. Scanning electron microscopy	16
4.2.5. Fourier transform infrared spectroscopy	16
4.2.6. Fluorescence spectroscopy	16
4.2.7. Site-selective fluorescence and kinetic spectroscopy	16
5. RESULTS AND DISCUSSION	18
5.1. Study of fluorescence self-quenching in the Nd^{3+} : LaF_3 bulk crystals	18
5.1.1. Theoretical background	18
5.1.2. Analysis of the impurity fluorescence self-quenching kinetics in LaF_3 crystals with low and medium concentration of Nd^{3+} ions	22
5.1.3. Analysis of the impurity fluorescence self-quenching kinetics in LaF_3 crystals with high concentration of Nd^{3+} ions	27
5.2. Study of the dependence of fluorescence quantum yield and brightness on concentration of dopant in aqueous colloidal solutions of Nd^{3+} : LaF_3 and Nd^{3+} : KY_3F_{10} nanocrystals	29
5.2.1. Theoretical background	30
5.2.2. Investigation of spectral and kinetic fluorescence properties of colloidal solutions of Nd^{3+} : LaF_3 and Nd^{3+} : KY_3F_{10} nanocrystals	33
5.2.3. Determination of the dependences on the concentration of the neodymium ion of the relative fluorescence quantum yield and brightness for aqueous colloidal solutions of Nd^{3+} : LaF_3 and Nd^{3+} : KY_3F_{10} nanocrystals	40

5.3. Investigation of substitution schemes of Ca^{2+} ions with impurity Nd^{3+} ions in the $\text{Ca}_3(\text{PO}_4)_2$ crystal lattice using laser site-selective and kinetic spectroscopy and DFT simulations.	42
5.3.1. Computational part	43
5.3.2. Laser site-selective and kinetic spectroscopy of the Nd^{3+} : β -TCP microceramics	46
5.3.3. Determination of the structure of the local environment of optical centers in Nd^{3+} : β -TCP microceramics	53
SUMMARY	56
SUMMARY IN ESTONIAN	58
ACKNOWLEDGEMENTS	60
REFERENCES	61
PUBLICATIONS	65
CURRICULUM VITAE	111
ELULOOKIRJELDUS	113

LIST OF PUBLICATIONS INCLUDED IN THE THESIS

- I. **E.A. Vagapova**, E. Strugovshchikov, E.O. Orlovskaya, A.S. Vanetsev, L. Dolgov, L. Puust, L.D. Iskhakova, U. Mäeorg, A. Pishtshev, Yu.V. Orlovskii, Combined spectroscopic and DFT studies of local defect structures in beta-tricalcium phosphate doped with Nd(III), *Journal of Alloys and Compounds*, 877, 2021, 160305.
- II. S.G. Fedorenko, A.V. Popov, **E.A. Vagapova**, A.E. Baranchikov, Yu.V. Orlovskii, Concentration self-quenching of luminescence in crystal matrices activated by Nd³⁺ ions: theory and experiment, *Journal of Luminescence*, 198, 2018, 138–145.
- III. Yu.V. Orlovskii, A.V. Popov, E.O. Orlovskaya, A.S. Vanetsev, **E.A. Vagapova**, M. Rähn, V. Sammelselg, I. Sildos, A.E. Baranchikov, P.V. Grachev, V.B. Loschenov, A.V. Ryabova, Comparison of concentration dependence of relative fluorescence quantum yield and brightness in first biological window of wavelengths for aqueous colloidal solutions of Nd³⁺: LaF₃ and Nd³⁺: KY₃F₁₀ nanocrystals synthesized by microwave-hydrothermal treatment, *Journal of Alloys and Compounds*, 756, 2018, 182–192.

Author's contribution

- I. Conceptualization, methodology, laser site-selective spectroscopy measurements, fluorescence kinetic measurement, experimental data processing, analysis of the experimental data, comparing calculated and experimental data, writing manuscript draft, review, and editing.
- II. Fluorescence kinetic measurements, analysis of the fluorescence self-quenching kinetics, participation in data processing, writing a part of the manuscript.
- III. Site-selective laser spectroscopy measurements, fluorescence kinetic measurements, participation in data processing, writing a part of the manuscript.

Other publications

- a) E. Vinogradova, L. Dolgov, V.A. Konyushkin, E.O. Orlovskaya, **E.A. Vagapova**, A. Treshchalov, V. Peet, V. Hizhnyakov, Yu.V. Orlovskii, Fluorescence of Nd³⁺ optical centers close to cubic symmetry in a calcium fluoride crystal co-doped with Na⁺, *Journal of Luminescence*, 234 (2021) 117988.

1. INTRODUCTION

Compounds of fluorides and complex phosphates are widely used in biomedicine due to their compatibility with biological tissues [1–4]. Doping of crystals of fluorides and complex phosphates with rare earth ions (RE) allows to expand their functions and add many useful properties [5–7]. In the form of nanoparticles, these materials can be used for various applications, such as visualization of biological tissues [8, 9], local heating of biological tissues [6, 8], non-invasive optical temperature measurement [10] etc. Micro- and nanoscale materials such as micro- and nanoparticles, as well as stable aqueous colloidal solutions of nanocrystals, are especially interesting for study.

Among the whole range of fluorescent RE ions for biomedical applications, the Nd^{3+} ion stands out. The main feature of this ion is that its spectral absorption lines at the $^4\text{I}_{9/2} \rightarrow ^4\text{F}_{5/2}$ and $^4\text{I}_{9/2} \rightarrow ^4\text{F}_{3/2}$ transitions, as well as the fluorescence spectral lines at the $^4\text{F}_{3/2} \rightarrow ^4\text{I}_{9/2}$ transition, lie in the transparency windows of biological tissues (so-called «biological windows»), which makes it possible to use materials doped with Nd^{3+} for non-invasive bioimaging of biological tissues at a depth of 1 cm [11]. Another important feature of the Nd^{3+} ion in crystalline matrices is that the $^4\text{F}_{3/2}$ level is a metastable energy level. This means that it has a relatively long lifetime, on the order of hundreds of microseconds, mainly determined by spontaneous radiative decay. This feature simplifies the detection of the fluorescence kinetics for its further analysis.

Materials doped with RE ions must necessarily have several properties in order to be used for biomedical applications, since they are intended to be introduced into the human organism:

1. Biocompatibility and lack of toxicity.

It is assumed that the material will be used in the human body; therefore, when administered, it should not cause any response from the immune system [12–14].

2. The size of the materials.

The required particle size will depend on the application, but it should be noted that this factor is important in the selection of the crystal matrix. On the one hand, it has been shown that the most optimal materials for bioimaging are luminescent nanoparticles doped by RE ions with an average size of less than 50 nm to provide the necessary cellular uptake and the clearance rate [14].

On the other hand, to control the survival rate of a biological implant, both a small size consisting of a biocompatible substance and a large implant covered with a thin layer of porous microceramic, for example, $\text{Ca}_3(\text{PO}_4)_2$, activated by RE ions can be used.

3. High values of brightness and fluorescence quantum yield.

Even with a low concentration of nanoparticles, it is necessary to ensure a sufficient brightness of the fluorescence.

Taking into account the above-mentioned condition for the absence of toxicity of materials used in biomedicine, the synthesis of biocompatible nano- and microparticles, as well as their colloidal solutions, is carried out by the so-called “soft” chemistry methods from aqueous solutions of salts [9, 15, 16]. These synthesis methods lead to the appearance of molecular OH⁻ groups in the volume of the synthesized materials, which cannot be completely removed from the crystal matrix, even during subsequent high-temperature annealing. The presence of molecular OH⁻ groups lead to enhanced quenching of the Nd³⁺ luminescence [9, 16, 17].

The main reason for the decrease in the fluorescence quantum yield and brightness of luminescent materials is the processes of nonradiative relaxation of the optical excitation energy. These nonradiative processes compete with spontaneous radiative decay and lead to a decrease in the intensity of the luminescent signal. The processes of nonradiative energy relaxation can be divided into intra- and inter-center relaxation. Nonradiative intra-center relaxation is the multiphonon relaxation in the optical center. Multiphonon relaxation is not considered in this work, since we are analyzing the fluorescence kinetics of the ⁴F_{3/2} level of Nd³⁺ ion, which has a large energy gap to the nearest lower-lying level ⁴I_{15/2} (on the order of 5000–6000 cm⁻¹ [18]). This means that the multiphonon relaxation has a very low probability and, therefore, makes a small contribution to the overall rate of nonradiative relaxation. Inter-center non-radiative relaxation processes imply nonradiative energy transfer between different optical centers. For the transfer of optical excitation energy to occur, it is necessary that there are excited ions, i.e. donors, and ions capable of accepting this energy, i.e. acceptors. In the general case, the transfer of optical excitation energy can occur when there is an overlap of the fluorescence spectral lines of donors and absorption spectral lines of acceptors. In the case of doping materials with RE ions, the same ion can be both a donor and an acceptor of energy. A small resonance mismatch between the energy levels of the donor and acceptor can be compensated by phonons of the crystal lattice.

At a low donor concentration, excitation cannot migrate over donor ions and, therefore, is quenched by acceptors at the place of origin. In this case, the fluorescence quenching is static and can be described by two successive quenching stages. At short times, we observe an exponential stage of ordered static decay, at which the fluorescence quenches on the nearest acceptors located in the first coordination sphere [19]. The ordered static stage is followed by the disordered Förster non-exponential stage of static quenching, which is characterized by quenching at more distant acceptors with uniform distribution [20, 21].

With an increase in the donor concentration, the migration of energy over donors to acceptors occurs and accelerates the quenching. The kinetics of impurity quenching ceases to be static, and its theoretical description becomes more complicated. In the general case, two different mechanisms of energy migration are possible in a system with a uniform distribution of donors: diffusion and hopping. The quenching mechanism is a hopping mechanism if

the average distance between donors is so large that the excitation is transferred to the so-called black sphere by one hop [22]. Otherwise, the quenching mechanism is diffusional, that is, the transfer of energy into the "black sphere" occurs due to many short hops, which is continuous diffusion. The limits of application of the hopping or diffusion model are determined by the relationship between C_{DA} (microparameter of donor-acceptor interaction) and C_{DD} (microparameter of donor-donor interaction). In crystal matrices doped with RE ions, in the overwhelming majority of cases, the hopping mechanism of energy transfer is realized.

The theory of hopping migration-accelerated self-quenching ($C_{DD} \gg C_{DA}$), consistently taking into account the correlation between migration and cross-relaxation processes, was proposed in [23, 24]. In these papers, the self-consistent method of diagrammatic summation of the Green density series functions proposed by Gushanur, Andersen, Fire (GAF) [25] and Loring, Andersen, Fire (LAF) [26] was used. However, as shown in [27], this method, which is successfully applied in the situation of migration-accelerated hopping quenching, gives incorrect results in the opposite diffusion limit and in the case of unsteady quasi-static quenching. The migration-accelerated stage of quasi-static quenching can be followed by a fluctuation stage. The fluctuation stage is associated with quenching in areas depleted of donors, that is, at isolated donor centers that appear due to concentration fluctuations [28]. The fluctuation stage of impurity quenching kinetics is similar to the Förster one but with a stronger decay [17, 28, 29]. It should be noted that the fluctuation stage can be observed both after the migration-accelerated stage of quenching, and immediately after the static (Förster) quenching stage, if the acceptors concentration is very high [17, 29].

On the one hand, nonradiative energy transfer is a negative process and reduces the brightness and fluorescence quantum yield. However, by analyzing the kinetics of impurity quenching, one can obtain additional information on the structure of the studied material. This method of materials structure analysis is called "energy transfer probe" and is used to analyze the local structure of crystal matrices doped with rare earth ions, see, i.e., [9]. By analyzing the fluorescence quenching kinetics, one can determine the fluorescence quenching mechanism, the dimension of the acceptor space, and draw conclusions about the structural and morphological reasons for the fluorescence quenching.

2. RESEARCH TASK

The main goal of the thesis is to study the radiative and nonradiative relaxation of optical excitation energy in crystalline matrices of different sizes, such as bulk crystals, microceramics and nanoparticles, doped with the Nd^{3+} ions, using laser site-selective and kinetic spectroscopy.

3. STATEMENTS PRESENTED FOR THE DEFENCE

The following statements are presented for the defense:

1. Measurement and analysis of the concentration dependence of the fluorescence impurity quenching kinetics in the Nd^{3+} : LaF_3 bulk crystals when only Nd-Nd self-quenching presents.
2. Measurement and analysis of the concentration dependences of the relative fluorescence quantum yield and brightness of aqueous colloidal solutions of Nd^{3+} : LaF_3 and Nd^{3+} : KY_3F_{10} nanoparticles, in presence of an additional channel of nonradiative energy transfer, namely, Nd^{3+} ions fluorescence quenching caused by OH^- molecular group vibrations.
3. The criteria for choosing a crystal matrix for doping with Nd^{3+} ions. Namely, a large ratio of the Judd-Ofelt intensity parameters Ω_4/Ω_6 , which leads to an increase in the luminescence branching ratio at the $^4\text{F}_{3/2} \rightarrow ^4\text{I}_{9/2}$ transition, and, consequently, to an increase in the luminescence intensity in the first biological window, as well as a small value of Ω_6 , which leads to a decrease in fluorescence concentration self-quenching and quenching by OH^- acceptors.
4. Types of charge compensation at heterovalent substitution of Nd^{3+} for Ca^{2+} ions in Nd^{3+} : β -TCP microceramics synthesized by water-based methods, and their effect on spectral and kinetic properties.
5. Determination of the relationship between the spectral and kinetic properties of the Nd^{3+} optical centers and their local crystalline environment, with the impurity fluorescence quenching kinetics analysis of Nd^{3+} : β -TCP ceramics as an example.

4. EXPERIMENTAL

4.1. Synthesis of the materials

In the framework of this study, materials of different sizes were used. Namely, a concentration series of Nd^{3+} : LaF_3 bulk crystals with a Nd^{3+} concentration in the range from 0.1 to 87.7 at. %; concentration series of colloidal solutions of Nd^{3+} : LaF_3 nanoparticles with Nd^{3+} concentration in the range from 0.1 to 43.6 at. %; concentration series of colloidal solutions of Nd^{3+} : KY_3F_{10} nanoparticles with Nd^{3+} concentration in the range from 0.1 to 2 at. %; Nd^{3+} : β -TCP microceramics with concentrations of Nd^{3+} ions 0.1 and 1 at. %.

4.1.1. Synthesis of the Nd^{3+} : LaF_3 bulk crystals

The LaF_3 single crystals of high optical quality activated by Nd^{3+} ions were grown from the melt by the descending crucible method in a fluorinating atmosphere.

4.1.2. Synthesis of the colloidal solutions of Nd^{3+} : LaF_3 and Nd^{3+} : KY_3F_{10} nanoparticles

The initial reagents used in the synthesis without any further purification include $\text{Nd}(\text{NO}_3)_3 \cdot 5\text{H}_2\text{O}$ (Aldrich, 99.999% purity), $\text{Y}(\text{NO}_3)_3 \cdot 4\text{H}_2\text{O}$ (Aldrich, 99.999% purity), $\text{La}(\text{NO}_3)_3 \cdot 6\text{H}_2\text{O}$ (99.999%), NH_4F (>98%) and KF (Aldrich, >99% purity).

4.1.2.1. Synthesis of the colloidal solutions of Nd^{3+} : LaF_3 nanoparticles

For the synthesis of aqueous colloidal solutions of Nd^{3+} : LaF_3 nanoparticles doped with (0.1-50 mol%) Nd^{3+} ions, $\text{La}(\text{NO}_3)_3 \cdot 6\text{H}_2\text{O}$ (0.4995-0.25 mmol) and $\text{Nd}(\text{NO}_3)_3 \cdot 5\text{H}_2\text{O}$ (0.0005-0.25 mmol) were dissolved in deionized water (15 mL). The solution of rare-earth salts was added dropwise to the NH_4F solution (5 mmol) in deionized water (25 mL) under vigorous stirring. To improve the dispersibility of the obtained nanoparticles, 1 g of biocompatible surfactant Polyvinylpyrrolidone (Aldrich, average $M_w \sim 55000$) was added to the rare-earth nitrates solutions before precipitation. The freshly precipitated gels were diluted with deionized water (10 mL) and left stirring for 15 min. The resulting solutions were transferred into a 100ml Teflon autoclave and placed under microwave irradiation for 2 h at 200 °C using a Speedwave Four (Berghof GmbH, Germany) laboratory device (2.45 GHz, 1 kW maximum output power). After they were cooled, centrifuged using a Thermo Scientific Heraeus Multi-

fuge X1 device and washed several times with deionized water. The resulting precipitates were redispersed in deionized water using ultrasonication.

4.1.2.2. Synthesis of the colloidal solutions of Nd³⁺: KY₃F₁₀ nanoparticles

For the synthesis of the aqueous colloidal solutions of the KY₃F₁₀ nanoparticles doped with Nd³⁺ ions (0.1, 1, and 2 mol%), Y(NO₃)₃•4H₂O (0.4995 mmol, 0.4950 mmol, and 0.4900 mmol) and Nd(NO₃)₃•5H₂O (0.0005 mmol, 0.0050 mmol, and 0.0100 mmol) were dissolved in 10ml of deionized water. The solution of rare-earth salts was added dropwise to the 5 mmol K₂F₂O solution under vigorous stirring. To improve the redispersibility of obtained nanoparticles, a biocompatible surfactant Polyvinylpyrrolidone (PVP) (Aldrich, average Mw ~55000) was added to the rare-earth nitrates solutions before precipitation. The freshly precipitated gels were diluted with deionized water (10 mL) and left stirring for 15 min. The resulting solutions were transferred into a 100ml Teflon autoclave and placed under microwave irradiation for 4 h at 200 °C using a Speedwave Four (Berghof GmbH, Germany) laboratory device (2.45 GHz, 1 kW maximum output power). After that they were cooled, centrifuged using a Thermo Scientific Heraeus Multifuge X1 device and washed several times with deionized water. The resulting precipitates were redispersed in deionized water using ultrasonication.

4.1.3. Synthesis of the Nd³⁺: Ca₃(PO₄) microceramics

The β-TCP samples were prepared by co-precipitation from water-ethanol system followed by annealing step at 800 °C for 2 h. Powder samples were synthesized with two levels of Nd³⁺ doping: 0.1 at. % and 1 at.%. Synthesis procedures use chemicals Ca(NO₃)₂•4H₂O, CaCl₂, (NH₄)₂HPO₄ (all three 99.9%, Reakhim), NH₄H₂PO₄ (99.9%, EuroChemicals), Nd₂O₃ (99.99%, Tailorlux), tartaric acid (99.99%, EuroChemicals), anhydrous ethanol (reagent grade), concentrated HNO₃ (reagent grade, EuroChemicals) and ammonia solution (25% solution, reagent grade, AppliChem) as a set of starting materials. To obtain the β-phase of TCP ceramics doped with Nd³⁺, we used a combination of chemical dissolution and precipitation methods. The synthesis began with the preparation of 30 mL of Ca(NO₃)₂ solution, which was obtained by dissolving 0.4675g of Ca(NO₃)₂•4H₂O in anhydrous ethanol. Thereafter, the desired amount of dopant (Nd³⁺) was introduced by adding Nd(NO₃)₃ solution, after which 10 mL of ammonium hydrophosphate solution prepared by dissolving 0.1761 g of (NH₄)₂HPO₄ in deionized water was admixed. The final reaction mixture was then allowed to stir for 1 h at room temperature. During stirring the pH = 9 was kept using an ammonia solution. The precipitate was centrifuged,

washed, placed in an oven and dried at 80 °C in air for 12 h. The dried powder was heat-treated at 800 °C in an oven for 2 h (heating rate of 10 °C/min).

4.2. Measurement technique

In this work, a variety of methods was used to characterize samples. Below are brief descriptions of each of them. A detailed description can be found in the respective publications.

4.2.1. Energy-dispersive X-ray spectroscopy

Concentration of Nd^{3+} ions in LaF_3 single crystals was determined by energy-dispersive X-ray spectroscopy (EDX) using the NVision 40 scanning electron microscope (Carl Zeiss) equipped with X-Max (Oxford Instruments) 80 mm² detector at 20 kV acceleration voltage. Before measurements, the samples were covered with carbon conducting layer.

FEI Titan Themis transmission electron microscope working at 200 kV was used to measure elements concentration in Nd^{3+} : LaF_3 and Nd^{3+} : KY_3F_{10} nanoparticles. Energy dispersive X-ray spectroscopy (EDX) signal of the nanoparticles was collected with SuperX silicon drift detector (Bruker) in TEM mode. Measurement parameters were set so that sample consisted only of La, Nd and F atoms. No chemical definition was used. Quantitative analysis was performed with Cliff-Lorimer method for F K-line; for La and Nd L-line using Bruker Esprit software. It provides accurate enough elemental analysis with high spatial resolution.

4.2.2. X-Ray diffraction analysis

The X-ray diffraction analysis of the synthesized nanoparticles Nd^{3+} : LaF_3 and Nd^{3+} : KY_3F_{10} was performed using a D/MAX 2500 diffractometer (Rigaku™, CuK α -radiation). The nanoparticles were studied in the powdered form after drying during several hours at 90 °C. The peaks were identified using the JCPDS database.

X-ray diffraction patterns of the 0.1 and 1 at. % Nd^{3+} : β -TCP samples were obtained on a Bruker D2 Phaser X-ray powder diffractometer with Cu K α radiation. Phase analysis and refinement of the lattice parameters were carried out using the software package DIFFRACplus (EVA and TOPAS 4.2.0.2).

4.2.3 Transmission electron microscopy

The transmission electron microscopy (TEM) images of the Nd^{3+} : KY_3F_{10} samples were taken with Leo912 AB Omega microscope under accelerating

voltage 100 kV. The colloid was placed on a TEM copper grid and dried for several hours.

4.2.4. Scanning electron microscopy

FEI Titan Themis 200 working at 200 kV was used for STEM images of concentration series of the Nd^{3+} : LaF_3 nanoparticles. Solutions were diluted in alcohol and ultrasonicated. Copper grids with carbon coating were used.

SEM images of the 0.1 and 1 at. % Nd^{3+} : β -TCP powders were obtained on a Tescan VEGA II SBU scanning electron microscope operated at an accelerating voltage of 5 kV in the backscattered electron recording mode.

4.2.5. Fourier transform infrared spectroscopy

Fourier transform infrared spectra of the 0.1 and 1 at. % Nd^{3+} : β -TCP were measured with Spectrum BXII (Perkin Elmer) FTIR spectrometer using ZnSe ATR (Interspectrum OÜ, Estonia), 6000 – 600 cm^{-1} , resolution 4 cm^{-1} .

4.2.6. Fluorescence spectroscopy

Detection of luminescence spectra of aqueous colloidal solutions of the Nd^{3+} : LaF_3 and Nd^{3+} : KY_3F_{10} nanocrystals in the spectral range of 800–1100 nm was carried out using the LESA-01-BIOSPEC® fiber optic spectrometer by excitation of the samples with a continuous laser diode at 804 nm (LPhT-800-01-BIOSPEC®), with a power density of 1 W/cm^2 . At the entrance slit of the spectrometer was put a BLP01-830R-25 Semrock filter blocking the laser radiation. To take into account the spectral sensitivity of the spectrometer, a calibration was carried out using a halogen light source LSH-4-BIOSPEC®.

4.2.7. Site-selective fluorescence and kinetic spectroscopy

The kinetics of the fluorescence decay of the $^4\text{F}_{3/2}$ level of Nd^{3+} ions in LaF_3 single crystals was detected at the $^4\text{F}_{3/2} \rightarrow ^4\text{I}_{9/2}$ transition using the single photon counting technique with MDR 23 monochromator (LOMO), a PMT Hamamatsu R636-10 and multichannel scaler (MCS) Timeharp 260 with nanosecond time resolution. The fluorescence of Nd^{3+} ions was excited by a pulsed Al_2O_3 -Ti laser LOTIS-TII LS-2134- LT40 ($f = 10$ Hz, $t_{\text{pulse}} = 8\text{--}30$ ns) directly into the $^4\text{F}_{5/2}$ level of the Nd^{3+} ions. Single crystals of Nd^{3+} : LaF_3 were placed relative to the laser beam in such a way as to excite luminescence of the middle part of the sample only, for which the concentration of Nd^{3+} ions were determined. To obtain fluorescence kinetics not distorted by various nonlinear processes, which can be summarized by the term “up-conversion”, we tried to reduce the energy

of the excitation pulse to a maximum possible value at which a further decrease in energy affected only the intensity of the kinetics, and not its form.

Site-selective fluorescence spectra and kinetics of the aqueous colloidal solutions of the Nd^{3+} : LaF_3 and Nd^{3+} : KY_3F_{10} nanocrystals were measured with excitation by a pulsed Al_2O_3 -Ti laser LOTIS-TII LS-2134-LT40 ($f = 10$ Hz, $t_{\text{pulse}} = 8\text{--}30$ ns) into the $^4\text{F}_{5/2}$ level of the Nd^{3+} ions. The fluorescence originated from the $^4\text{F}_{3/2}$ level of Nd^{3+} ions was dispersed by MDR 23 monochromator (LOMO) with 0.1 nm spectral resolution. The longpass filter FEL0850 (Thorlabs) was attached to its front slit to block the laser radiation. The fluorescence was detected at the $^4\text{F}_{3/2} \rightarrow ^4\text{I}_{9/2}$ transition of Nd^{3+} ions by single photon counting technique with PMT Hamamatsu R636-10 and multichannel scaler (MCS) Timeharp 260 (PicoQuant GmbH) with nanosecond time resolution.

To measure the site-selective fluorescence spectra of the 0.1 and 1 at. % Nd^{3+} : β -TCP, all samples were excited by a pulsed Rhodamine 6G dye laser DL-Compact (Estla Ltd., Estonia) with laser line width $\Delta\lambda = 0.02$ nm at FWHM pumped by the second harmonics of Nd: YAG (model LQ215, $f = 20$ Hz, pulse duration 5 ns, Solar laser systems, Belarus). The fluorescence was dispersed with an Andor Shamrock SR303i spectrometer and recorded with a gated Andor Technology iCCD camera iStar DH320T-18H-13. BLP01-808R-25 edge-filter (Semrock) was attached to the front slit of the monochromator to prevent the penetration of stray light resulting from laser excitation. Fluorescence kinetics was detected using a Hamamatsu PMT 6240-02 operating in the gated photon-counting mode and equipped with a multi-channel analyzer (Fast Comtec P7882) with a time resolution of 100 ns. The samples were cooled in a helium bath cryostat (Kyiv, Ukraine), which allowed the samples to be cooled to 4.2 K.

5. RESULTS AND DISCUSSION

5.1. Study of fluorescence self-quenching in the Nd³⁺: LaF₃ bulk crystals

A key feature of bulk fluoride crystals doped with RE ions is the absence of additional acceptors in the volume, namely molecular OH⁻ groups, whose vibrations cause significant quenching of the RE ions fluorescence [9]. The presence of such acceptors leads to the appearance of an additional fluorescence quenching channel and complicates the theoretical modeling of the fluorescence kinetics of impurity quenching. Modeling the kinetics, when there is only one channel of nonradiative transfer of electronic excitation energy, namely Nd*-Nd self-quenching, is the first step towards solving the problem of fluorescence quenching of rare earth ions in nanocrystals. As model object, we used a concentration series of Nd³⁺ – doped LaF₃ crystals, in which there is only one channel of nonradiative energy transfer. Thus, we were able to compare the theoretical modeling of the kinetics of impurity fluorescence self-quenching in the presence of Nd-Nd concentration self-quenching only with real experimental kinetics.

5.1.1. Theoretical background

To study the mechanisms of fluorescence self-quenching, we analyzed the fluorescence impurity quenching kinetics $N(t)$ obtained from the measured fluorescence kinetics $I(t)$ by dividing it by the kinetics describing spontaneous radiative decay

$$N(t) = I(t)/\exp(-t/\tau_R) \quad (1)$$

To determine the lifetime of spontaneous radiative decay τ_R , the fluorescence kinetics of a sample with a minimum impurity content is usually measured. We assume that at a minimum impurity concentration in the crystal, the processes of nonradiative transfer of electronic excitation energy make a minimal contribution to the fluorescence decay kinetics, and at the far stage, the fluorescence decay kinetics is approximated by an exponential function with a decay constant corresponding to τ_R .

The mechanisms of resonance energy migration and self-quenching of the excited $^4F_{3/2}$ level of the Nd³⁺ ion is dipole-dipole, since all transitions involved in cross-relaxation processes are forced electro-dipole transitions. Migration of electronic excitation energy occurs as a result of the cross-relaxation at the $^4F_{3/2} \rightarrow ^4I_{9/2}$; $^4I_{9/2} \rightarrow ^4F_{3/2}$ transitions and self-quenching as a result of the cross-relaxation at the $^4F_{3/2} \rightarrow ^4I_{15/2}$; $^4I_{15/2} \rightarrow ^4I_{9/2}$ transitions. All these transitions have the square of the reduced matrix element $U^{(2)} = 0$ [30] that means the absence of

the quadrupole part of the optical transition in both the donor and the acceptor. We also disregard the contribution of magnetic dipole-dipole mechanism of energy transfer for the $^4F_{3/2}$ level of the Nd^{3+} , since magnetic dipole transitions are allowed only for transitions with $|\Delta J| \leq 1$, but not for $0 \rightarrow 0$ transitions. This does not apply to cross-relaxation transitions.

When analyzing the self-quenching kinetics in $LaF_3:Nd^{3+}$ bulk crystals, we use the probabilities $u(r)$ and $w(r)$ of the dipole-dipole interaction between Nd^{3+} ions in the case of migration and cross-relaxation of the electronic excitation energy, which are described by the following expressions

$$U(r) = \frac{C_{DD}}{r^6}, \quad w(r) = \frac{C_{DA}}{r^6} = z \frac{C_{DD}}{r^6}, \quad z = C_{DA}/C_{DD}. \quad (2)$$

As a result, the expression for the fluorescence self-quenching kinetics $N(t)$ takes the form [23, 24]

$$N(t) = e^{-a^2 t} (a - b)^{-1} [a e^{a^2 t} \operatorname{erfc}(a\sqrt{t}) - b e^{b^2 t} \operatorname{erfc}(b\sqrt{t})] \quad (3)$$

$$a = \frac{[\Delta_A + \Delta_D \eta(z)]}{2}; \quad b = \frac{[\Delta_A - \Delta_D \eta(z)]}{2}; \quad \eta(z) = \sqrt{1 + z/2} - \sqrt{z/2} \quad (4)$$

$$\Delta_A = (2\pi^2/3)\rho\sqrt{C_{DA}}; \quad \Delta_D = (2\pi^2/3)\rho\sqrt{C_{DD}} \quad (5)$$

ρ – concentration of donor centers (Nd^{3+} ions), $[nm^{-3}]$

In the case of a uniform and equiprobable distribution of the acceptors in the bulk crystal when averaging over the rates of donor-acceptor interactions with different distances in a donor-acceptor pair, at short times $t \ll \Delta_D^{-2}$, the kinetics (3) in case of dipole-dipole donor-acceptor interaction can be represented as Förster function

$$N(t) = \exp(-\gamma_A t^{1/2}) \quad (6)$$

$$\gamma_A = \frac{4}{3} \pi^{3/2} \rho \sqrt{C_{DA}} \quad (7)$$

where γ_A – is a macroparameter of energy transfer.

The behavior of kinetics (3) at long times is determined by the parameter b . Excitation migration prevails over cross-relaxation processes at negative values of the parameter b , when the following relation is valid

$$b < 0 \rightarrow \frac{\sqrt{2z}}{(\sqrt{1+z/2} - z/2)} < 1 \rightarrow z < 0.25 \quad (8)$$

As can be seen from conditions (8), this occurs at sufficiently small z . Under these conditions, kinetics (3) shows an exponential decay, describing the migration-accelerated stage of self-quenching

$$N(t) \approx [1 - \Delta_A/\Delta_D \eta(z)] \exp[-\Delta_A \Delta_D \eta(z)t]; \quad t \gg \Delta_D^{-2} \quad (9)$$

At the migration-accelerated stage of self-quenching (for hopping quenching), the decay of kinetics occurs according to a simple exponential law with a rate

$$\overline{W} = \Delta_A \Delta_D \eta(z) = \frac{2\sqrt{2}\pi^4}{9} \rho^2 \sqrt{C_{DA}C_{DD}} \eta(z) \quad (10)$$

The function $\eta(z)$ in the hopping migration mechanism ($z = C_{DA}/C_{DD} \rightarrow 0$) tends to infinity and decreases monotonically with increasing z . It describes the effect of correlation between the processes of self-quenching and resonance migration and is reflected in self-quenching rate W . The boundary time between the initial Förster stage of static quenching and the migration-accelerated stage is defined as

$$t_s = \frac{32\eta^2(z)}{\pi\gamma_D^2} \quad (11)$$

In crystals and glasses doped with Nd^{3+} ions, as a rule, the resonant migration of optical excitations dominates over cross-relaxation processes; since the parameter z is sufficiently small, and the fluorescence self-quenching kinetics is described by expressions (9), (10). In this case, the Förster stage of static quenching (6) is rather short and can be hidden behind the initial exponential ordered stage. It is important to note that a decrease in the Nd^{3+} concentration does not lead the kinetics to purely static Förster quenching.

Formula (3) correctly describes the fluorescence self-quenching kinetics only for sufficiently small z for which inequality (8) is satisfied. Small values of the parameter z in the case of self-quenching mean that the migration of excitation occurs according to the hopping mechanism [31, 32], while the main decay of the kinetics due to rapid migration has an exponential form (9), with the quenching rate (10). However, in the regions of the crystal depleted of donors, the migration of excitation slows down due to the large distances between the donor sites. Consequently, the migration accelerated quenching kinetics should sooner or later be replaced by delayed nonstationary quenching of the excitations of donors trapped in these regions of the crystal. The fluctuation stage of the impurity fluorescence quenching kinetics can be described by the following expression

$$N^0(t) = \exp\{-\gamma_A \sqrt{(1 + 1/z)t}\} = \exp\{-\gamma_D \sqrt{(1 + z)t}\} \quad (12)$$

where $\gamma_A = \frac{2}{\sqrt{\pi}} \Delta_A = \frac{4}{3} \pi^{3/2} \rho \sqrt{C_{DA}}$ и $\gamma_D = \frac{2\sqrt{2}}{\sqrt{\pi}} \Delta_D = \frac{4}{3} \pi^{3/2} \rho \sqrt{C_{DD}}$ – macroparameters of static self-quenching and energy migration, respectively.

In the range of small values of z ($z \ll 1$), the migration-accelerated hopping self-quenching, described by formulas (3), (6), and (9), is realized over a sufficiently long initial time interval. However, sooner or later, exponentially decaying kinetics (9) transforms into the fluctuation stage of hopping self-quenching (12). The time when the fluctuation stage begins is defined as the point of intersection of the kinetics of the migration-accelerated stage (9) and the kinetics of the fluctuation stage ($N^0(t)$) (12)

$$t_f = \frac{8}{\pi \Delta_A^2} \frac{(1 + z)}{\eta^2(z)} = \frac{32}{\pi^2 \gamma_A^2} \frac{(1 + z)}{\eta^2(z)} \quad (13)$$

Comparing this time with the start time t_s of the exponential stage (11), we obtain the relation

$$\frac{t_s}{t_f} = \pi \frac{z}{1 + z} \eta^4(z) \quad (14)$$

As follows from (14), the ratio of the boundary times depends only on the parameter z and does not depend on the donor concentration. For small z values, this ratio is linear. Accordingly, the smaller z is, the later the fluctuation stage of the impurity quenching kinetics begins and the more excitations are quenched at the migration-accelerated stage of hopping self-quenching. At small z , after the decomposition of the radical in (12), the fluctuation self-quenching kinetics takes the following form

$$N(t) \approx N^0(t) \approx \exp\left\{-\gamma_D \sqrt{t} - \frac{\sqrt{z}}{2} \gamma_A \sqrt{t}\right\}, \quad t \gg t_f, \quad z \ll 1 \quad (15)$$

Thus, using the above theoretical description of the impurity quenching kinetics, we can solve two problems, direct and inverse. The direct problem is to simulate the fluorescence impurity quenching kinetics of various materials doped with RE ions without performing an actual experiment. Solving the inverse problem, using a detailed analysis of the fluorescence impurity quenching kinetics, we can determine the mechanisms of fluorescence quenching, the dimensions of the donor and acceptor spaces, and draw conclusion about the origin of the fluorescence quenching processes. In practice, the inverse problem is usually implemented.

5.1.2. Analysis of the impurity fluorescence self-quenching kinetics in LaF₃ crystals with low and medium concentration of Nd³⁺ ions

Usually, the processing of the experimentally obtained concentration fluorescence self-quenching kinetics begins with the determination of the donor-acceptor interaction microparameter C_{DA} . In the general case, in the stepwise analysis of the impurity quenching kinetics, this parameter can be found in two ways:

1. Analysis of the disordered (Förster) stage of the impurity self-quenching kinetics, which is determined by expression (6).

This method is traditional and has a high accuracy in determining the parameter γ_A in the presence of a deep section of the Förster quenching. However, in the presence of strong migration-accelerated quenching, the Förster stage of static quenching is very short, and it is difficult to correctly determine the γ_A macroparameter. In our case, there is no second acceptor and therefore we only take into account self-quenching of the Nd – Nd luminescence; therefore, the migration-accelerated process of nonradiative energy transfer is pronounced. According to formula (3), with a change in the impurity concentration, kinetic changes are not observed if the parameter z does not change.

2. Analysis of the initial ordered stage of the static quenching kinetics, which has an exponential form and is determined by the expression

$$N(t) = \exp(-W_{ord}t), \quad t \ll t_1 \quad (16)$$

In the case when the disordered static stage is very short and quickly changes to the migration-accelerated stage, it becomes impossible to determine the C_{DA} microparameter from it. In this case, it is possible to determine the interaction microparameter C_{DA} from an ordered static stage, the rate of which depends on it linearly:

$$W_{ord} = c_D C_{DA} P, \quad P = \sum_i r_{1i}^{-6} \quad (17)$$

where c_D – is relative donor concentration.

The boundary time t_1 between ordered static quenching and the Förster stage for strongly dilute solid solutions does not depend on the impurity concentration, but depends exclusively on C_{DA} and the volume Ω occupied by one site of the donor sublattice

$$t_1 = \Omega^2 / C_{DA} \quad (18)$$

On the side of long times, the interval of the disordered stage of kinetics is limited by the boundary time t_s (11), which is inversely proportional to the square of donor concentration.

In expression (17), the summation is performed over all sites of donor sublattice, except for the initially excited site. This method has such disadvantages as the low accuracy of C_{DA} determination at low concentrations. It should be noted that in concentrated systems this method is the only one since the entire kinetic curve is described by ordered decay exponent.

The rate of ordered decay is determined from an analysis of the impurity fluorescence self-quenching kinetics. To determine it, according to expression (1), it is necessary to determine the lifetime of the spontaneous radiative decay τ_R . Usually, the lifetime of spontaneous radiative decay is determined for a sample with a low concentration of impurity in order to minimize the influence of non-radiative energy transfer. In our case, we studied a sample with an Nd^{3+} ion concentration of 0.1 at. % (Fig. 1, upper curve). Approximating the far stage of its fluorescence kinetics by a decaying exponential function, we determined the spontaneous decay lifetime $\tau_R = 701 \mu\text{s}$. The impurity fluorescence quenching kinetics was obtained according to (1) by division of fluorescence kinetics to kinetics of exponential decay with $\tau_R = 701 \mu\text{s}$ (Fig. 2).

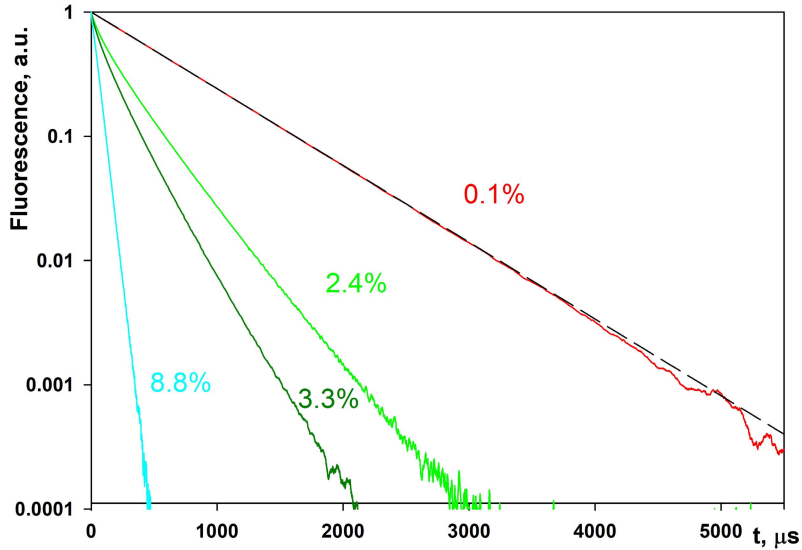


Fig. 1. Fluorescence kinetics in bulk crystal $\text{LaF}_3:\text{Nd}^{3+}$ under excitation at 803 nm wavelength and fluorescence detection at 863.2 nm wavelength depending on Nd^{3+} concentration – broken curves. Fitting by exponential decay with $\tau_R = 701 \mu\text{s}$ – dashed line.

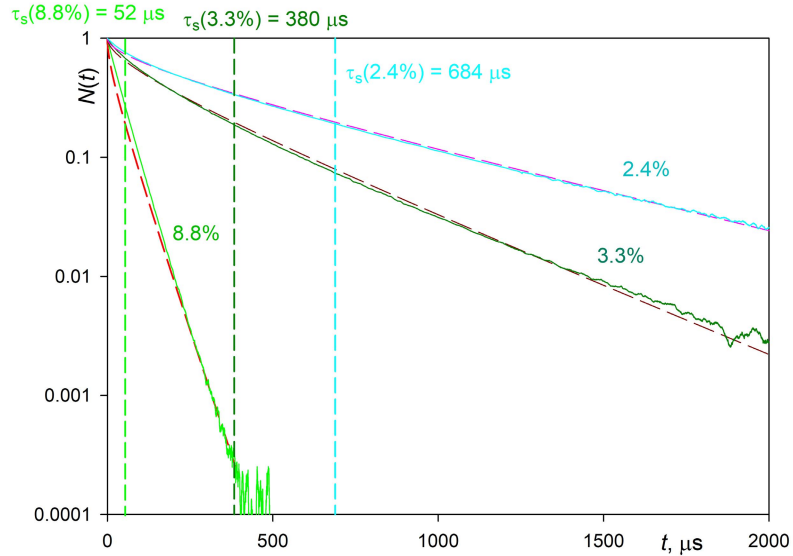


Fig. 2. Concentration dependence of the impurity quenching kinetics of Nd^{3+} ions in $\text{LaF}_3:\text{Nd}^{3+}$ crystals. Dotted curves – theoretical calculation.

Self-quenching of luminescence occurs in the volume of the crystal. As shown earlier, in the case of a donor-acceptor dipole-dipole interaction, the Förster stage of static luminescence quenching is described by expressions (6, 7). We can determine whether there is a Förster stage of static quenching by the presence of linear sections with a slope angle with $\text{tg}\varphi = 1/2$ in the impurity quenching kinetics, replotted in the coordinates $\lg(-\ln(N(t)))$ vs. $\lg t$ (Fig. 3). The analysis of the presented kinetic curves shows that the static Förster stage of the fluorescence quenching is absent in the studied samples. An additional confirmation of the absence of a disordered Förster stage, according to expression (6), is the absence of a linear section on the kinetic curves replotted in coordinates $\ln(N(t))$ vs. $t^{1/2}$ (Fig. 4).

The presence of an ordered static stage of fluorescence quenching is determined by presence of a linear section with a slope $\text{tg}\varphi = 1$ in the quenching kinetics replotted in $-\lg(-\ln(N(t)))$ vs. $\lg t$ coordinates (Fig. 3) that follows from expression (16). The presence of an ordered stage of static quenching, as well as its rate, can be confirmed by rearranging the fluorescence impurity quenching kinetics in the coordinates $\ln(N(t))$ vs. t (Fig. 4). It follows from expression (16) that the linear part slope of the fluorescence impurity self-quenching kinetics, replotted in the coordinates $\ln(N(t))$ vs. t (Fig. 5), will determine the rate of ordered static quenching. For the studied concentration series of LaF_3 crystals, the static quenching rates are: $W_{ord}(2.4\%) = 0.0064 \mu\text{s}^{-1}$, $W_{ord}(3.3\%) = 0.00985 \mu\text{s}^{-1}$ и $W_{ord}(7.6 - 9.7\%) = 0.054 \mu\text{s}^{-1}$. For the LaF_3 crystal, the lattice sum is $P = 2400 \text{ nm}^{-6}$ [33].

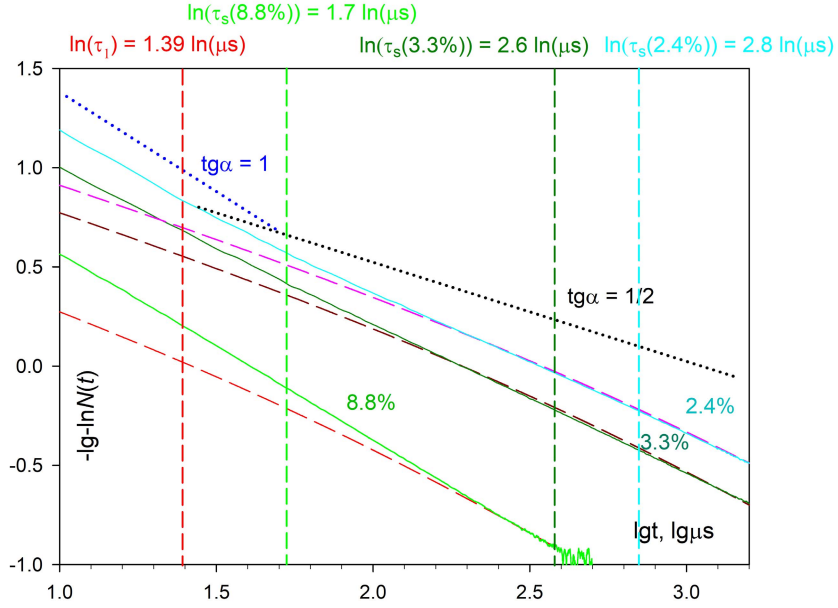


Fig. 3. Concentration dependence of the impurity quenching kinetics of Nd^{3+} ions and its theoretical calculation (dashed curves) for $\text{LaF}_3:\text{Nd}^{3+}$ crystals, plotted in special coordinates.

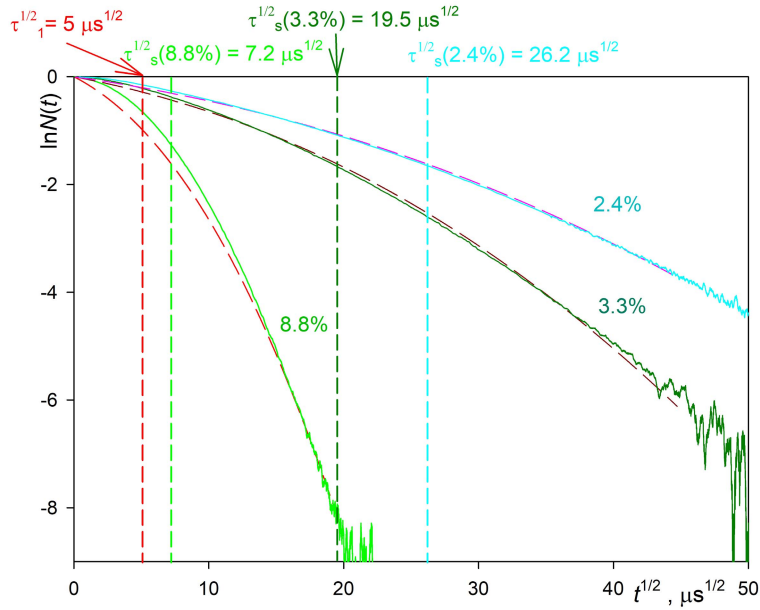


Fig. 4. Concentration dependence of the impurity quenching kinetics of Nd^{3+} ions and its theoretical calculation (dashed curves) for $\text{LaF}_3:\text{Nd}^{3+}$ crystals, plotted in special coordinates.

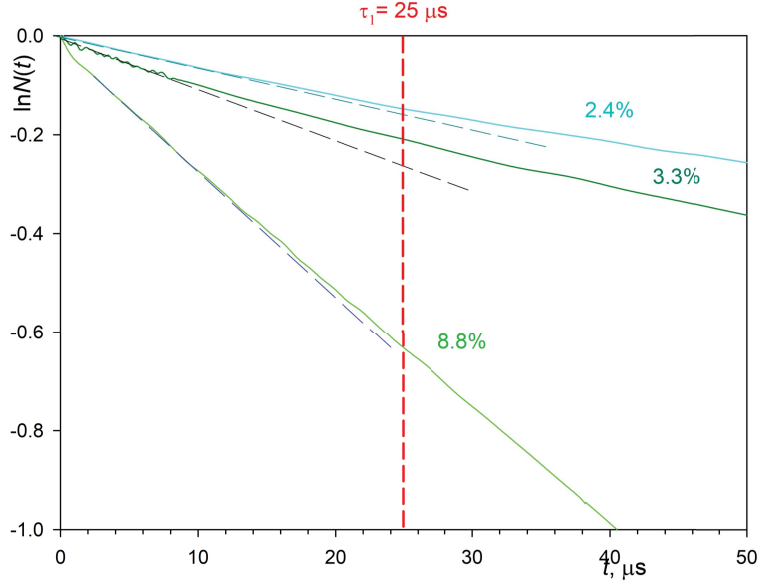


Fig. 5. Concentration dependence of the ordered static stage of the impurity quenching kinetics of Nd^{3+} ions in $\text{LaF}_3:\text{Nd}^{3+}$ crystals. Dotted curves – theoretical calculation.

Using these data, we calculated the microparameter C_{DA} for the initial ordered static stage of (eq. 17). The result for different impurity concentrations gives an insignificant spread in the values: $C_{DA} = 0.11; 0.13; 0.125 \text{ nm}^6/\text{ms}$.

Direct fitting of the kinetics according to formula (3) gives the best agreement between the experimental and calculated data for the Nd^{3+} concentrations of 2.4% and 3.3% at $C_{DA} = 0.13 \text{ nm}^6/\text{ms}$, $C_{DD} = 0.85 \text{ nm}^6/\text{ms}$ ($z = 0.15$). For these values of microparameters, an ideal coincidence of theoretical and experimental curves is achieved (Fig. 2–5). An exception is a small initial part of the non-stationary kinetics after the end of ordered decay, in which the theory predicts a short section of static quenching, which is absent in experiment. It should be noted that, during the fitting process, the selected C_{DA} value is primarily responsible for the curvature of the initial self-quenching stage up to times $t \sim t_s$, while the C_{DD} value forms the kinetic curvature mainly at the final stage of the kinetic curve. This makes the fitting procedure rather unambiguous. In general, having the concentration series of kinetic curves and determining (by fitting) the C_{DA} and C_{DD} values for several curves simultaneously, it is possible to check the correctness of determination of neodymium concentration in the entire series of samples. The accuracy of determining the concentration by the kinetic method significantly exceeds the accuracy of other methods. For the kinetic data of the third sample, measurements by the non-kinetic EDX method gave an estimate range 7.6–9.7%. Using the selected values of microparameters and concentration, at which the best coincidence of

the calculated and experimental curves is achieved, we obtained a value of 8.8% (Fig. 2–5). Note that, for this concentration the mismatches between experiment and theory are more noticeable at the initial stage of kinetics. This is due to the system going beyond the limits of the continuous medium model $R \gg R_{\min}$, when the distance between the donor and acceptors can approach R_{\min} that is not taken into account in formula (3).

Now, knowing the energy transfer microparameters, we can calculate the boundary times for various stages of the kinetics of impurity self-quenching. Using expression (18) and the value $\Omega = 0.0566 \text{ nm}^3$ for the elementary volume of the donor sublattice [34] for the LaF_3 lattice, we obtain $t_l = 25 \text{ }\mu\text{s}$ (Fig. 5, red dashed line). Accordingly, in the interval $t < 25 \text{ }\mu\text{s}$, the impurity quenching kinetics includes only an ordered stage of fluorescence static quenching.

As follows from formula (11), the boundary time t_s depends on concentration and the parameter z . Expression (11) gives the values $t_s = 684 \text{ }\mu\text{s}$, $t_s = 380 \text{ }\mu\text{s}$, $t_s = 52 \text{ }\mu\text{s}$ for concentrations (2.4%, 3.3%, 8.8%), respectively (Fig. 2–4). Calculating the boundary time t_f of the fluctuation stage using formula (13), we have: $t_f = 4930 \text{ }\mu\text{s}$, $t_f = 2738 \text{ }\mu\text{s}$, $t_f = 376 \text{ }\mu\text{s}$.

As follows from relation (14), the ratio of t_s and t_f does not depend on the concentration but depends only on the parameter $z = C_{DA}/C_{DD}$. So, for $z = 0.15$ at any concentration $t_f = 7.2t_s$. In fact, the main decay in the observed kinetics at all three concentrations occurs mainly at the migration-accelerated stage of self-quenching (9), (10). With an increase in the neodymium concentration to 8.8%, the boundary of the measured interval almost reaches t_f . Further, at $t \gg t_f$, the kinetics should change from fast exponential quenching (9), (10) to slow fluctuation decay (15).

5.1.3. Analysis of the impurity fluorescence self-quenching kinetics in LaF_3 crystals with high concentration of Nd^{3+} ions

The above analysis of the impurity fluorescence self-quenching kinetics is not suitable for highly concentrated systems. With an increase in the neodymium concentration, the rate of the migration-accelerated stage \bar{W} (10), which increases according to the quadratic law with increasing donor concentration, sooner or later becomes greater than the maximum possible self-quenching rate W_{ord} , which linearly depends on the donor concentration. In this case, the multistage self-quenching kinetics transforms into single stage ordered decay (16), (17). The critical concentration of neodymium ions c_D^* , at which this transition occurs, is determined by the relation

$$\bar{W}(c_D^*) = W_{ord}(c_D^*), \rightarrow c_D^* = 0.033\Omega^2 P\sqrt{z}/\eta(z) \quad (19)$$

The critical concentration depends on the lattice constants of the crystal and is an increasing function of the parameter z up to the limiting values of the existence of migration-accelerated stage, determined by inequality (8) ($z = 0.25$).

Substituting the value $\Omega^2 P = 7.695$ of the dimensionless lattice sum for LaF_3 and the value $z = 0.15$ determined by fitting, we obtain the value of the critical concentration of neodymium in the crystal: $c_D^* = 12.6\%$.

We measured the fluorescence decay kinetics for crystals with a high impurity content (Fig. 6). All measured kinetic curves are described by exponential decay with times $\tau = 12.1, 6.1, 4.3$ and $3.1 \mu\text{s}$ for concentrations of 27.0%, 50.4%, 60.0%, and 87.7%, respectively.

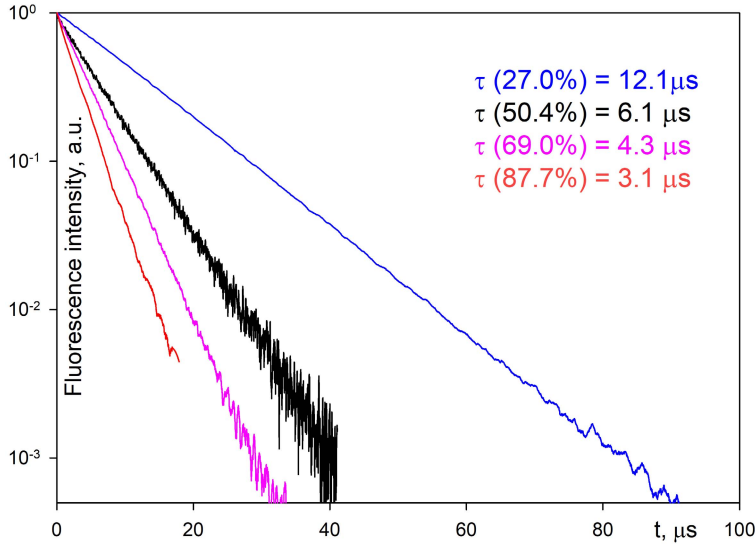


Fig. 6. Concentration dependence of the impurity self-quenching kinetics in $\text{Nd}^{3+}:\text{LaF}_3$ crystals at a high impurity concentration.

This exponential decay corresponds to the ordered stage of fluorescence static self-quenching (16), which means that using expression (17), we can calculate the microparameter $C_{DA} = 0.128, 0.136, 0.140$ и $0.153 \text{ nm}^6/\text{ms}$.

With an increase in the Nd^{3+} concentration from 50% and more, an increase in the microparameter of energy transfer C_{DA} is observed, which in the general case should be a constant characteristic of the system. This growth can be explained by two factors. The first factor is an increase in the crystal field strength due to a slight decrease in the parameters of the crystal lattice under the conditions of the predominance of the NdF_3 structure over the LaF_3 structure. This leads to an increase in the line strength of electric dipole transitions S_{ED} in the Nd^{3+} ion and, as a consequence, to an increase in the C_{DA} and C_{DD} microparameters, according to the theory [35]. Another factor is the different values of the lattice sum P for LaF_3 and NdF_3 . The difference in the lattice constants of LaF_3 ($a = 7.367 \text{ \AA}$; $c/a = 1.025$) and NdF_3 ($a = 7.021 \text{ \AA}$; $c = 7.196$) is about 2.3%. This increases the lattice sum P for NdF_3 in comparison with LaF_3 by

15.5% and gives the value $C_{DA} = 0.132 \text{ nm}^6/\text{ms}$ at 87.7% Nd^{3+} , which is in qualitative agreement with the value obtained from the kinetic fit for low Nd^{3+} concentrations.

5.2. Study of the dependence of fluorescence quantum yield and brightness on concentration of dopant in aqueous colloidal solutions of Nd^{3+} : LaF_3 and Nd^{3+} : KY_3F_{10} nanocrystals

Fluoride nanoparticles doped with Nd^{3+} ions have been repeatedly tested to visualize biological tissues at a depth of one centimeter [7, 8]. Bioimaging in the “first biological window” (750–950 nm) is the easiest, since it is possible to use low-noise and low-cost detectors in this range [8]. In this regard, an urgent problem is the choice of a crystal matrix for the synthesis of nanoparticles doped by Nd^{3+} ions with the maximum fluorescence brightness in the “first biological window”. It may seem that the easiest way to do this is to choose the matrix with the highest absorption cross section σ_A at the $^4\text{I}_{9/2} \rightarrow ^4\text{F}_{5/2}$ transition ($\sim 800 \text{ nm}$) and the highest radiative spontaneous emission probability A at the $^4\text{F}_{3/2} \rightarrow ^4\text{I}_{9/2}$ transition ($\sim 860\text{--}870 \text{ nm}$). However, along with an increase in the absorption of laser radiation and the intensity of luminescence, in accordance with the Förster – Dexter theory [20, 36], the rate of energy transfer from the excited donor (Nd^{3+} ion) to the quenching acceptor will also increase, which will lead to degradation of the luminescence characteristics. We can distinguish two main quenching channels in nanocrystals doped with Nd^{3+} ions, which are synthesized by water methods: co-precipitation (CO) and hydrothermal microwave treatment (HTMW) [15]. The first is $\text{Nd}^*\text{-Nd}$ self-quenching, the contribution of which to the impurity quenching kinetics increases with an increase in the concentration of neodymium ions. The second channel is the fluorescence quenching as a result of nonradiative energy transfer to third-party acceptors. For nanoparticles synthesized by water methods, this is a quenching channel on molecular OH^- groups, which makes a significant contribution to the fluorescence impurity quenching kinetics [9, 16, 17].

Thus, the choice of the crystal matrix for fluorescent nanoparticles doped with Nd^{3+} ions for bioimaging in the near-IR spectral range can be approached in different ways. On the one hand, to increase the fluorescence intensity, one can try to synthesize well-crystallized defect-free binary fluoride nanocrystals, for example, a YF_3 crystal with a high spontaneous decay rate ($\tau_R = 390 \text{ } \mu\text{s}$ [37]). In this case, it is also necessary to provide a low concentration of dopant in order to reduce the contribution of self-quenching, as well as a low volume content of OH^- molecular groups in order to reduce quenching. The latter is hardly achievable using “green” water synthesis. In addition, the low concentration of Nd^{3+} reduces the luminescence intensity. Another way is to use crystal host matrices with a reduced line strength S_{ED} of the transitions and,

therefore, with reduced self-quenching and quenching caused by vibrations of molecular OH⁻ groups. The relationship between spontaneous emission rate A and the rate of fluorescence quenching affects the choice of the optimal concentration of impurity Nd³⁺ ions required to achieve the maximum fluorescence brightness. In other words, this relationship determines the maximum Nd³⁺ concentration, at which an increase in the luminescence intensity with an increase in the impurity concentration still prevails over its decrease as a result of concentration self-quenching (due to nonradiative (quenching) energy transfer).

In this part of the work, we tried to establish the criteria for choosing a crystal matrix for nanoparticles doped with Nd³⁺ ions to provide the maximum fluorescence intensity (maximum branching ratio) at the ${}^4F_{3/2} \rightarrow {}^4I_{9/2}$ transition, that is, in the “first biological window” with a minimum fluorescence self-quenching and quenching on third-party acceptors.

5.2.1. Theoretical background

In order to compare the fluorescence intensity of the ${}^4F_{3/2} \rightarrow {}^4I_{9/2}$ transition for two different crystal matrices doped with Nd³⁺ ions, it is necessary to compare the parameters in the expression

$$I(t) = n^*(t)A\beta_{1j}h\left(\frac{1}{\lambda_{1j}}\right), \quad (20)$$

where n^* is the population of the excited level ${}^4F_{3/2}$; A is the rate of spontaneous radiative decay from an excited level, which is the sum of the rates $\sum_j A_{1j}$ over all transitions to the lower lying manifolds of the Nd³⁺ ion; β_{1j} is the fluorescence branching ratio from the ${}^4F_{3/2}$ manifold to one of the lower lying level $j - {}^4I_{9/2}, {}^4I_{11/2}, {}^4I_{13/2}, {}^4I_{15/2}$ manifolds j ; $h\left(\frac{1}{\lambda_{1j}}\right)$ is the transition energy. The probability of a radiative transition depends on the line-strength of the electric-dipole transition S_{ED} as [35]

$$A(J_a - J_{a'}) = \frac{64e^2\pi^4}{3h} \left(\frac{1}{\lambda_{aa'}^3}\right) \chi_{ED} \frac{1}{(2J_a + 1)} S_{ED}^{aa'} \quad (21)$$

where

$$\chi_{ED} = \frac{n(n^2 + 2)^2}{9} \quad (22)$$

and

$$S_{ED}^{aa'} = \sum_{k=2,4,6} \Omega_k U_{aa'}^{(k)} \quad (23)$$

where Ω_k and $U^{(k)}$ are the intensity parameters and squares of the reduced matrix elements of Judd-Ofelt theory, respectively [38, 39].

In order to increase the fluorescence branching ratio β_{1j} for the ${}^4F_{3/2} \rightarrow {}^4I_{9/2}$ ($j = \frac{9}{2}$) transition by decreasing the line-strength S_{ED} for the ${}^4F_{3/2} \rightarrow {}^4I_{11/2}$ transition and increasing the line-strength S_{ED} for the ${}^4F_{3/2} \rightarrow {}^4I_{9/2}$, it is necessary to choose a crystal matrix with a large value of Ω_4 and a small value of Ω_6 ($\Omega_4 > \Omega_6$), since for the ${}^4F_{3/2} \rightarrow {}^4I_{9/2}$ transition $U^{(4)} > U^{(6)}$, while for the ${}^4F_{3/2} \rightarrow {}^4I_{11/2}$ transition, the opposite situation is observed (Table 1 [30]).

If the condition ($\Omega_4 > \Omega_6$) is satisfied, then the rates of the remaining transitions from the ${}^4F_{3/2}$ level of the Nd^{3+} ion also decreases, since for the ${}^4F_{3/2} \rightarrow {}^4I_{13/2}$ and ${}^4F_{3/2} \rightarrow {}^4I_{15/2}$ transitions the matrix element $U^{(4)} = 0$. This additionally increases the branching ratio at the ${}^4F_{3/2} \rightarrow {}^4I_{9/2}$ transition. For two promising fluoride matrices for doping with Nd^{3+} ions, LaF_3 и KY_3F_{10} , the ratios ($\Omega_4 > \Omega_6$) are 1.03 and 0.55, respectively. It can be assumed that the fluorescence branching ratio β_{1j} , and, consequently, the fluorescence intensity for the ${}^4F_{3/2} \rightarrow {}^4I_{9/2}$ transition for Nd^{3+} : LaF_3 will be higher than for Nd^{3+} : KY_3F_{10} .

Table 1. The calculated squares of reduced matrix elements for some electronic transitions of the Nd^{3+} ion [30] responsible for fluorescence intensity and fluorescence quenching.

Transition	$U^{(2)}$	$U^{(4)}$	$U^{(6)}$
${}^4F_{3/2} \rightarrow {}^4I_{9/2}$	0	0.2293	0.0548
${}^4F_{3/2} \rightarrow {}^4I_{11/2}$	0	0.1136	0.4104
${}^4F_{3/2} \rightarrow {}^4I_{13/2}$	0	0	0.2085
${}^4F_{3/2} \rightarrow {}^4I_{15/2}$	0	0	0.0288
${}^4I_{9/2} \rightarrow {}^4I_{15/2}$	0	0.0001	0.0453
${}^4I_{9/2} \rightarrow {}^4F_{5/2}$	0.0010	0.2371	0.3972
${}^4I_{9/2} \rightarrow {}^4H(2)_{9/2}$	0.0092	0.008	0.1155

The rate of dipole-dipole energy transfer W_{DA} from the donor (excited Nd^{3+} ion) to the acceptor (unexcited Nd^{3+} ion) is proportional to the product of the line-strengths S_{ED}^D and S_{ED}^A of energy resonance transitions in the donor and acceptor, as well as to the overlap integral S of their luminescence and absorption spectra [35]

$$W_{DA}^{dd} = \frac{1}{(2J_D + 1)(2J_A + 1)} \left(\frac{2}{3}\right) \left(\frac{2\pi}{\hbar}\right) \left(\frac{e^2}{R^3}\right)^2 \left(\sum_{k=2,4,6} \Omega_{kD} U_{aa'D}^{(k)} \right) \times \left(\sum_{k=2,4,6} \Omega_{kA} U_{aa'A}^{(k)} \right) S \quad (24)$$

Based on the above formula, it can be seen that to decrease the rate of fluorescence quenching W_{DA} , it is necessary to find a crystal matrix for doping with Nd^{3+} ions, with a reduced value of the line strength S_{ED} for transitions in the donor and acceptor involved in the resonant cross-relaxation process. Self-quenching of the ${}^4\text{F}_{3/2}$ level is determined by the ${}^4\text{F}_{3/2} \rightarrow {}^4\text{I}_{15/2}$ transition in the donor ($U^{(4)} = 0$, $U^{(6)} = 0.0288$) and the ${}^4\text{I}_{9/2} \rightarrow {}^4\text{I}_{15/2}$ transition in acceptor ($U^{(4)} = 0.0001$ и $U^{(6)} = 0.0453$). To reduce self-quenching, it is also necessary to choose a crystal matrix with a small value of Ω_6 , regardless of the Ω_2 and Ω_4 values, because of zero or almost zero values of the matrix elements $U^{(2)}$ and $U^{(4)}$ for the ${}^4\text{F}_{3/2} \rightarrow {}^4\text{I}_{15/2}$ transition in the donor and ${}^4\text{I}_{9/2} \rightarrow {}^4\text{I}_{15/2}$ in the acceptor, respectively.

Besides, all transitions from the ${}^4\text{F}_{3/2}$ level can participate in cross-relaxation nonradiative energy transfer to vibrational levels of molecular OH^- groups [40]. The most effective resonant nonradiative energy transfer from an excited neodymium ion to OH^- acceptors occurs at low resonance energies, i.e. involving the ${}^4\text{F}_{3/2} \rightarrow {}^4\text{I}_{15/2}$ и ${}^4\text{F}_{3/2} \rightarrow {}^4\text{I}_{13/2}$ transitions in the donor. And in this case, we should only care about a low value of the intensity parameter $\Omega^{(6)}$ to ensure a low line-strength S_{ED} for the transition in the Nd^{3+} donor, and thereby reduce the efficiency of cross-relaxation transitions between excited Nd^{3+} ions and OH^- acceptors, because both matrix elements $U^{(2)}$ and $U^{(4)}$ for these transitions are equal to zero (Table 1).

Table 2. The intensity parameters Ω_k , indices of refraction n in the near IR, and spontaneous emission lifetimes τ_R for several Nd^{3+} doped fluoride bulk crystals, which can be employed for water-based synthesis of the same nanocrystals for near IR bioimaging.

Crystal host	Ω_2 , 10^{-20} cm^2	Ω_4 , 10^{-20} cm^2	Ω_6 , 10^{-20} cm^2	Ω_4/Ω_6	n	τ_R , μs
LaF_3	0.35	2.57	2.50	1.03	1.5693	701 [41]
KYF_4	0.86	2.39	3.93	0.61	1.41	714 [42]
KY_3F_{10}	1.37	4.16	7.56	0.55	1.48	550 [43]
LiYF_4	1.9	2.7	5.0	0.54	1.45	550 [44]
LiLuF_4	1.19	1.27	4.04	0.31	1.468	495 [45]
LiKYF_5	0.92	3.21	4.26	0.75	1.45	475 [46]
$\alpha\text{-NaYF}_4$	6.07	3.05	10.52	0.29	1.467	330 [47]

We may assume that the fluorescence quenching for Nd^{3+} : KY_3F_{10} will be stronger than for Nd^{3+} : LaF_3 because parameter Ω_6 for the Nd^{3+} : LaF_3 crystal is three times less, 2.50×10^{-20} [48], as compared to the Nd^{3+} : KY_3F_{10} , $7.56 \times 10^{-20} \text{ cm}^2$ [45].

To verify the correctness of our preliminary conclusion, based on the estimation of the ratio of the intensity parameters Ω_4/Ω_6 and the values of Ω_6 in bulk crystals, below we compared the measured concentration dependences of the relative fluorescence quantum yield (FQY) η for aqueous colloidal solutions of $\text{Nd}^{3+}:\text{LaF}_3$ и $\text{Nd}^{3+}:\text{KY}_3\text{F}_{10}$ nanoparticles associated with the quenching energy transfer to acceptors [49]

$$\eta = \frac{1}{\tau_R} \int_0^{\infty} I(t)/I(0)dt \quad (25)$$

where $I(t)$ is measured fluorescence kinetics.

Also, for aqueous colloidal solutions of $\text{Nd}^{3+}:\text{LaF}_3$ и $\text{Nd}^{3+}:\text{KY}_3\text{F}_{10}$ nanocrystals, we compared the concentration dependence of the fluorescence brightness (FB), which is the product of FQY η and the absolute impurity concentration n_D [nm^3] (Brightness = $\eta \times n_D$).

5.2.2. Investigation of spectral and kinetic fluorescence properties of colloidal solutions of $\text{Nd}^{3+}:\text{LaF}_3$ and $\text{Nd}^{3+}:\text{KY}_3\text{F}_{10}$ nanocrystals

The ratio of the areas under the spectral fluorescence bands for two transitions $^4\text{F}_{3/2} \rightarrow ^4\text{I}_{9/2}$ and $^4\text{F}_{3/2} \rightarrow ^4\text{I}_{11/2}$ of Nd^{3+} ion of aqueous colloidal solutions of 3 at. % $\text{Nd}^{3+}:\text{LaF}_3$ (Fig. 7, black curve) and 1 at. % $\text{Nd}^{3+}:\text{KY}_3\text{F}_{10}$ (Fig. 7, red curve) nanocrystals (NCs) at room temperature, measured upon excitation by a tunable laser with a wavelength of 800 nm and a spectral resolution of 4 nm, corrected for the spectral sensitivity of the setup, confirm our assumption that the fluorescence branching ratio at the $^4\text{F}_{3/2} \rightarrow ^4\text{I}_{9/2}$ transition is higher for the $\text{Nd}^{3+}:\text{LaF}_3$ nanocrystals than for $\text{Nd}^{3+}:\text{KY}_3\text{F}_{10}$ nanocrystals due to the larger Ω_4/Ω_6 ratio for the former.

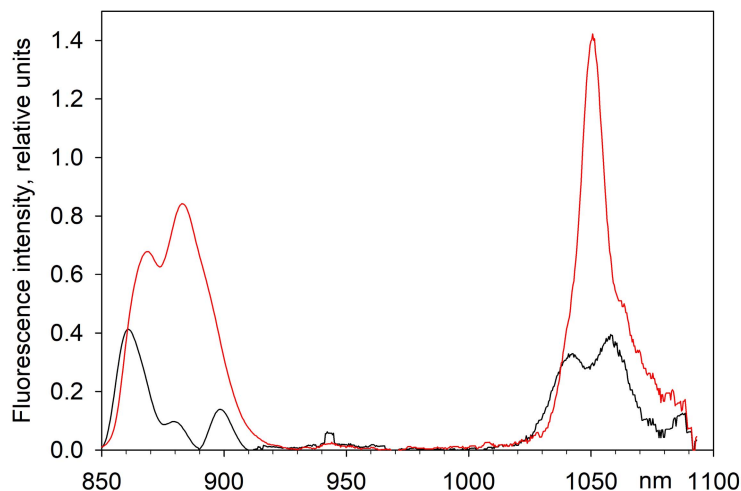


Fig. 7. Fluorescence spectra of aqueous colloidal solutions of NCs at room temperature with excitation at a wavelength of 804 nm and measurements at a spectral resolution of 4 nm. The spectra are corrected taking into account the spectral sensitivity of the setup. The left spectral line belongs to the $^4F_{3/2} \rightarrow ^4I_{9/2}$ transition, and the right one belongs to $^4F_{3/2} \rightarrow ^4I_{11/2}$ transition of Nd^{3+} . A 3 at. % Nd^{3+} : LaF_3 – black spectrum and 1 at. % Nd^{3+} : KY_3F_{10} – red spectrum.

5.2.2.1. Kinetic fluorescence spectroscopy of colloidal solutions of Nd^{3+} : LaF_3 nanocrystals

There is an intense narrow spectral line at a wavelength of 862.8 nm at the fluorescence spectrum of an aqueous colloidal solution of 1 at. % Nd^{3+} : LaF_3 , measured at the $^4F_{3/2} \rightarrow ^4I_{9/2}$ transition with a spectral resolution of 0.1 nm, which is associated with the inter-Stark transition $^4F_{3/2}(1) \rightarrow ^4I_{9/2}(1)$ (Fig. 8). The excitation was carried out at a wavelength of 803 nm in the "first biological window". The shape of the fluorescence spectrum is the same as that of a bulk crystal, which indicates good crystallization of the synthesized nanoparticles. The measured fluorescence kinetics of an aqueous colloidal solution of Nd^{3+} : LaF_3 nanoparticles demonstrates strong quenching with an increase in the Nd^{3+} ion concentration from 0.1 to 43.6 at. % (Fig. 9).

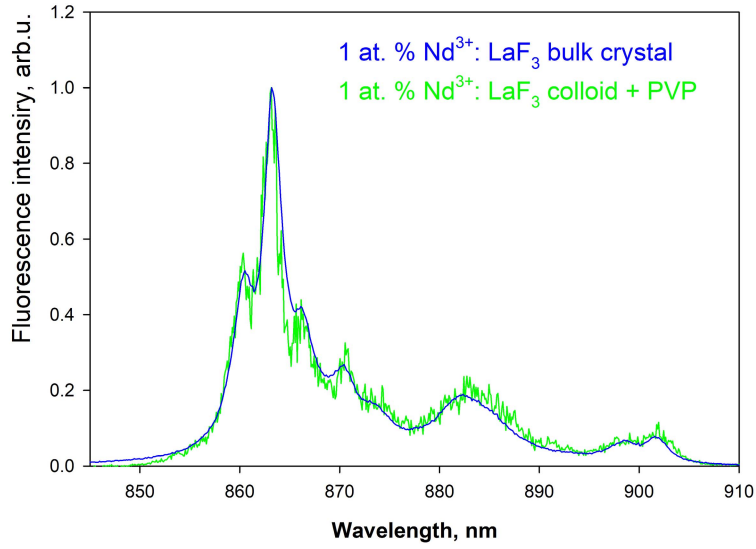


Fig. 8. The measured fluorescence spectra of the 1 at. % Nd^{3+} : LaF_3 bulk crystal and for aqueous colloidal solution of the 1 at. % Nd^{3+} : LaF_3 NCs at 300 K in first biological window ($^4\text{F}_{3/2} \rightarrow ^4\text{I}_{9/2}$ transition).

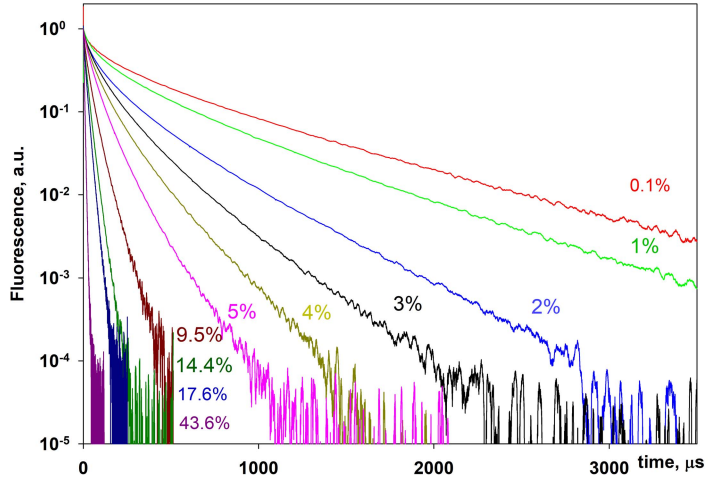


Fig. 9. Fluorescence kinetics of aqueous colloidal solutions of Nd^{3+} : LaF_3 NCs at room temperature with various dopant concentrations, excited at 803 nm and detected at 862.8 nm.

To determine the relative luminescence quantum yield FQY from the measured fluorescence kinetics $I(t)$ according to Eq. (25), it is necessary to determine the radiative lifetime τ_R . For this, it is necessary to minimize the impurity quenching

of the fluorescence. Therefore, we measured the fluorescence kinetics in the sample with the minimum content of the impurity RE ion.

Comparison of the fluorescence decay kinetics of the ${}^4F_{3/2}$ level of the Nd^{3+} ion in an aqueous colloidal solution of LaF_3 nanocrystals at a relative concentration of Nd^{3+} ions of 1 at. % synthesized with PVP, and a bulk crystal with the same impurity concentration, demonstrated their significant difference (Fig. 10). If the kinetics of a bulk crystal decays exponentially with $\tau_R = 701 \mu\text{s}$ [41], then the kinetics of a colloidal solution does not initially decrease exponentially, but exponentially decays at a late stage with a radiative lifetime $\tau_R = 750 \mu\text{s}$. The nonexponential decay at the initial stage of the kinetics is associated with the nonradiative transfer of optical excitation energy to the vibrations of OH^- molecular groups located in the volume of nanoparticles.

It should be taken into account that the lifetime of an excited level associated only with spontaneous radiative transitions to states with lower energies is different in a bulk crystal and in a colloidal solution of nanocrystals for the same crystal matrix. The ratio of the spontaneous radiative decay lifetime for a crystal and nanoparticles is proportional to the ratio of the refractive index of the medium in which the nanoparticles are located to the refractive index of the crystal [50]. The spontaneous radiative decay lifetime for a colloidal solution of $\text{Nd}^{3+}:\text{LaF}_3$ nanoparticles in PVP will be longer than for an $\text{Nd}^{3+}:\text{LaF}_3$ bulk crystal since the refractive index of the medium in which nanoparticles are located is less than the refractive index of the crystal.

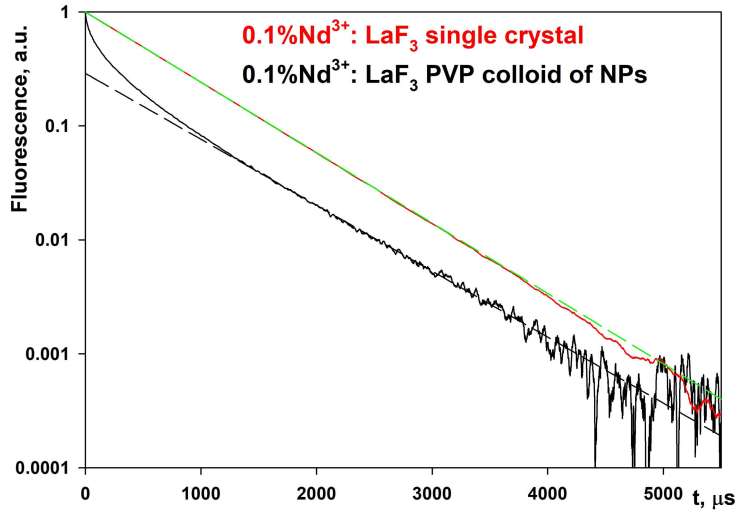


Fig. 10. Fluorescence decay kinetics of the ${}^4F_{3/2}$ level of the Nd^{3+} ions in a bulk LaF_3 crystal at a concentration of Nd^{3+} $c = 0.1$ at. % (red curve) and an aqueous colloidal solution of 0.1 at. % $\text{Nd}^{3+}:\text{LaF}_3$ nanocrystals with PVP (black curve). Approximation by exponential function $\exp(-t/\tau_R) = 701 \mu\text{s}$ is green dashed line; $\tau_R = 750 \mu\text{s}$ is the black dashed line.

5.2.2.2. Site-selective laser spectroscopy of the aqueous colloidal solutions of Nd^{3+} : KY_3F_{10} nanoparticles

Determination of the dependence of the relative fluorescence quantum yield of an aqueous colloidal solution of Nd^{3+} : KY_3F_{10} nanocrystals at room temperature on Nd^{3+} concentration is hampered by the presence of two types of optical centers (OC) [49]. In this case, it was necessary to study Nd^{3+} : KY_3F_{10} nanoparticles by laser site-selective spectroscopy to determine the true fluorescence kinetics for each type of optical centers, and then the true value of the relative fluorescence quantum yields and brightness.

Site-selective time-resolved fluorescence spectra of a colloidal solution of 1 at. % Nd^{3+} : KY_3F_{10} nanoparticles were measured at room temperature with different excitation wavelengths of 575, 801.9 and 857 nm (Fig. 11, black, red, and green, respectively). The spectra show fluorescent transitions for two types of optical centers in accordance with the energy levels diagram [49]. The arrows mark the inter-Stark transitions for two types of optical centers. The legend for identifying the inter-Stark transitions OC1 and OC2 is on the graph.

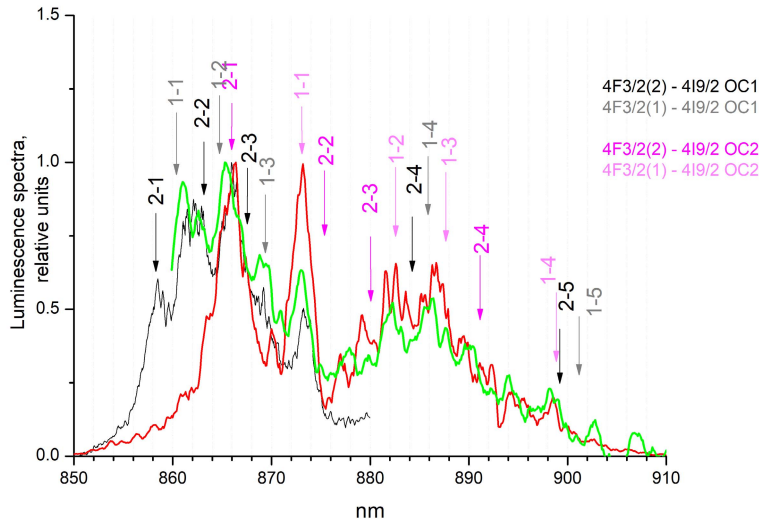


Fig. 11. Site-selective fluorescence spectra of an aqueous colloidal solution of the 0.1 at. % Nd^{3+} : KY_3F_{10} NCs at room temperature with different excitation wavelengths: 575 nm – black; 801.9 nm – red; 857 nm – green. Arrows mark inter-manifold inter-Stark transitions for two types of optical centers. A legend for identifying optical transitions of OC1 and OC2 is on the graph.

Using the methods of site-selective laser and kinetic spectroscopy, we were able to identify the fluorescence kinetics for two types of optical centers (Fig. 9) and measure its concentration dependence (Figs. 13 and 14).

First, we determined the spontaneous emission lifetime for OC1 by measuring the selective fluorescence kinetics of an aqueous colloidal solution of 0.1 at. % Nd^{3+} : KY_3F_{10} nanoparticles at room temperature at an excitation wavelength of 861.0 nm and a detection wavelength of 857.5 nm in the anti-Stokes region in order to reduce the contribution from the scattered light of the exciting laser ($\tau_R = 761 \mu\text{s}$) (Fig. 12, upper curve) and for OC2, at excitation wavelength of 801.9 nm and detection of 873.0 nm ($\tau_R = 447 \mu\text{s}$) (Fig. 12, lower curve). The kinetics measured at an excitation wavelength of 801.7 nm and recorded at a wavelength of 857.5 nm is the sum of the fluorescence kinetics of two types of optical centers (Fig. 12, middle curve).

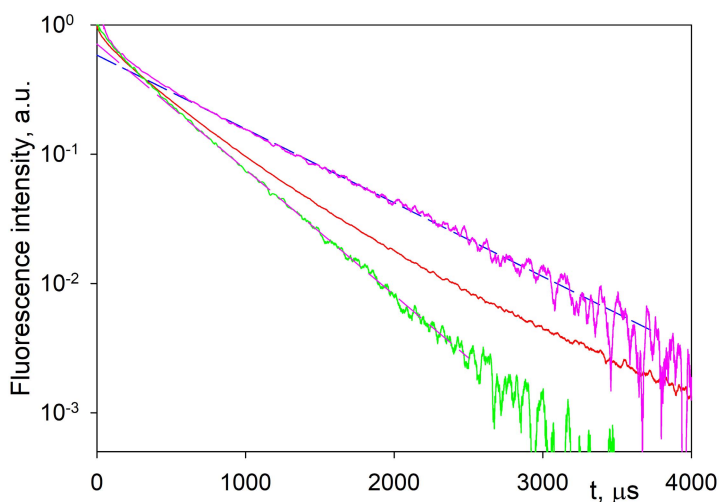


Fig. 12. Site-selective fluorescence kinetics of an aqueous colloidal solution of 0.1% Nd^{3+} : KY_3F_{10} NCs at room temperature: upper solid curve – OC1, excitation 861 nm, detection 857.5 nm; bottom solid curve – OC2, excitation 801.9 nm, detection 873 nm; middle solid curve – excitation 801.7 nm, detection 857.5 nm, a sum of two optical centers. Dashed curves correspond to exponential decay: $\tau_R = 761 \mu\text{s}$ – upper, blue; and $\tau_R = 447 \mu\text{s}$ – bottom, pink.

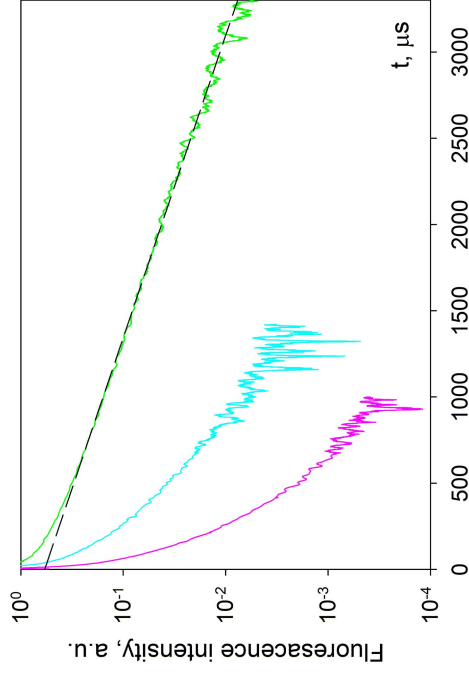


Fig. 13. Site-selective fluorescence kinetics of **OC1** of aqueous colloidal solutions of Nd^{3+} : KY_3F_{10} NCs at room temperature versus neodymium concentration. Fluorescence is excited at 861 nm directly at the $^4\text{F}_{3/2}$ level and detected at 857.5 nm in anti-Stokes region. From top to bottom $c = 0.1\%$ (green), 1% (cyan), and 2% (pink). The dashed line is an exponential decay with $\tau_R = 761 \mu\text{s}$.

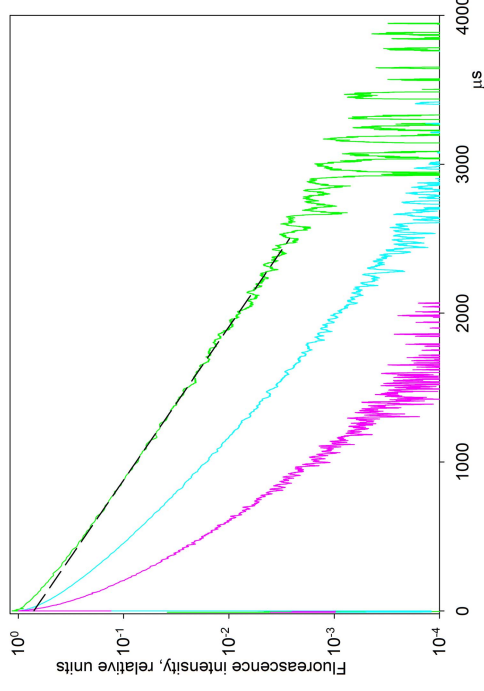


Fig. 14. Site-selective fluorescence kinetics of **OC2** of aqueous colloidal solutions of Nd^{3+} : KY_3F_{10} NCs at room temperature versus neodymium concentration. Fluorescence is excited at 801.9 nm at the $^4\text{F}_{5/2}$ level and detected at 873 nm. From top to bottom $c = 0.1\%$ (green), 1% (cyan), and 2% (pink). The dashed line is an exponential decay with $\tau_R = 447 \mu\text{s}$.

5.2.3. Determination of the dependences on the concentration of the neodymium ion of the relative fluorescence quantum yield and brightness for aqueous colloidal solutions of Nd^{3+} : LaF_3 and Nd^{3+} : KY_3F_{10} nanocrystals

We used the measured dependence of the fluorescence kinetics on the concentration of neodymium ions to plot a similar concentration dependence of the relative fluorescence quantum yield FQY (formula 25) of aqueous colloidal solutions of Nd^{3+} : LaF_3 nanocrystals associated with quenching energy transfer to unexcited Nd^{3+} ions and molecular OH^- groups. The FQY decreases monotonically with an increase in the Nd^{3+} concentration (Fig. 15, left, blue curve). At the same time, the fluorescence brightness calculated as the product of FQY and the absolute concentration of Nd^{3+} in $[\text{nm}^{-3}]$ (Fig. 15, right, blue curve) first increases to 3 at. % of Nd^{3+} ions, and with a further increase in concentration, it begins to decrease monotonically. Plateau between 5 and 9.5 at. % Nd^{3+} for colloidal solutions of Nd^{3+} : LaF_3 nanoparticles may have a physical reason associated with the fluorescence quenching (Nd^*-Nd self-quenching and quenching by the second acceptor (OH^- groups)), accelerated by energy migration over Nd^{3+} ions.

The selective relative FQY for aqueous colloidal solutions of (0.1, 1, 2 at. %) Nd^{3+} : KY_3F_{10} nanocrystals at room temperature, associated with the optical excitation energy transfer, was calculated as the area under the measured fluorescence kinetics normalized to the maximum divided by the measured spontaneous emission lifetime $\tau_R = 761 \mu\text{s}$ for OC1 and $\tau_R = 447$ for OC2. For OC1, FQY rapidly decreases, approximately 20 times with an increase in the Nd^{3+} concentration from $c = 0.001$ (0.0138 nm^{-3}) to $c = 0.02$ (0.276 nm^{-3}) (Fig. 15, left, pink curve), although for 0.1 at. % Nd^{3+} : KY_3F_{10} FQY even more than for 0.1 at. % Nd^{3+} : LaF_3 . At the same time the fluorescence brightness reaches a maximum already at $c = 0.01$ (0.138 nm^{-3}) and then rapidly decreases (Fig. 15, right, pink curve). At $c = 0.02$ (0.038 nm^{-3}), it drops to almost the same value as observed for $c = 0.001$. Thus, a smooth decrease in FQY and a pronounced maximum of FB are observed with an increase in the concentration of neodymium ions in both systems. However, for OC1 in Nd^{3+} : KY_3F_{10} nanocrystals, this drop begins at a concentration that is four times lower than for Nd^{3+} : LaF_3 (1 and 4 at. %, respectively). We attribute this to higher rates of nonradiative energy transfer, which lead to stronger $\text{Nd}-\text{Nd}$ self-quenching and $\text{Nd}-\text{OH}$ quenching in the first case.

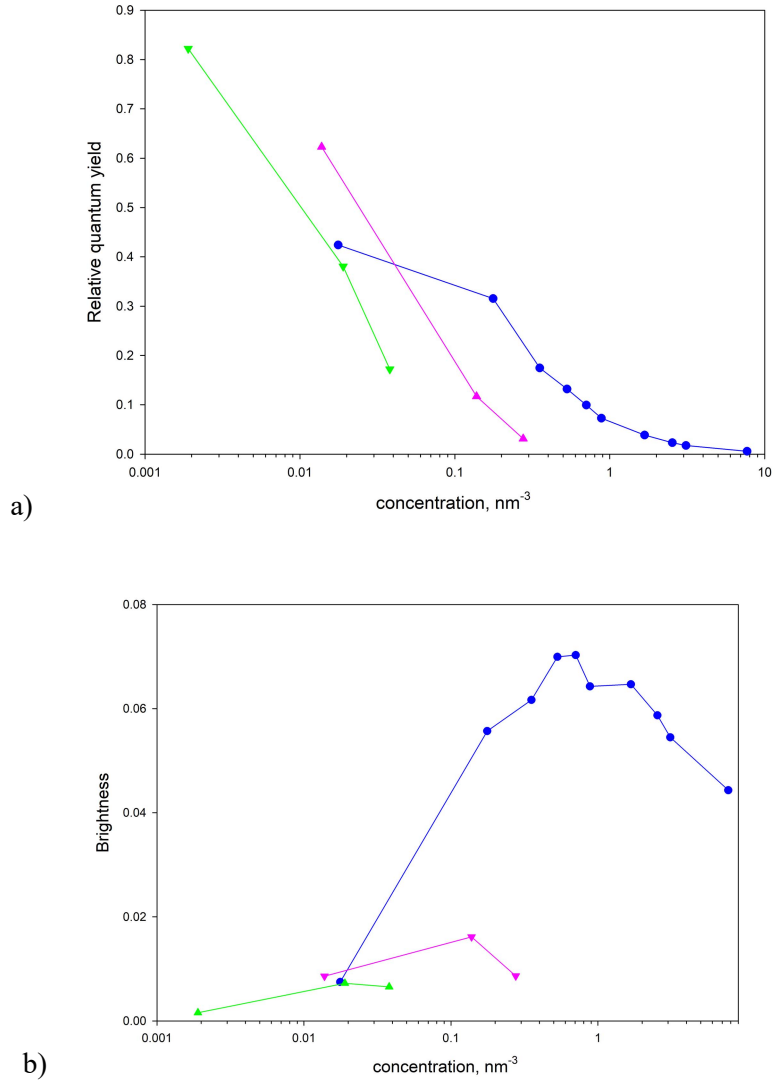


Fig. 15. The relative fluorescence quantum yield η (Eq. (7)) (a) and the fluorescence brightness (relative fluorescence quantum yield $\eta \times n_D$, absolute concentration of Nd^{3+}) (b) on n_D for aqueous colloidal solutions of the Nd^{3+} : LaF_3 and Nd^{3+} : KY_3F_{10} NCs at room temperature. Nd^{3+} : LaF_3 – circles, blue; Nd^{3+} : KY_3F_{10} – OC1 – down-triangles, pink; OC2 – up triangles, green.

This result is in qualitative agreement with our theoretical estimate of the fluorescence quenching in two crystal matrices doped with Nd^{3+} ions. We predicted stronger quenching in Nd^{3+} : KY_3F_{10} than in Nd^{3+} : LaF_3 , due to the higher value of Ω_6 (Table 2). Selective relative FQY of OC2 in an aqueous colloidal solution of 0.1 at. % Nd^{3+} : KY_3F_{10} nanoparticles is even higher than

for OC1, but also very quickly, about 20 times, decreases with an increase in the Nd^{3+} concentration from $c = 0.001$ ($1.9 \cdot 10^{-3} \text{ nm}^{-3}$) to $c = 0.02$ (0.038 nm^{-3}), and the fluorescence brightness also has a maximum at $c = 0.01$ (0.019 nm^{-3}). The fluorescence brightness of OC2 is much weaker than for OC1, due to more than 7 times lower value of its absolute concentration [49].

5.3. Investigation of substitution schemes of Ca^{2+} ions with impurity Nd^{3+} ions in the $\text{Ca}_3(\text{PO}_4)_2$ crystal lattice using laser site-selective and kinetic spectroscopy and DFT simulations

Various methods are available to study the crystal structure of materials, including XRD, FTIR, and solid-state NMR. Analysis of the fluorescence impurity quenching kinetics («energy transfer probe») is a promising method for observing the features of the local crystal structure. This method requires samples doped with rare earth ions, e.g., with Nd^{3+} ions [9]. The method is very sensitive and can be used to determine the local crystal structure in combination with data obtained by other methods. However, for the full use of this method, it is necessary to study in detail the inhomogeneous splitting of spectral lines in the material in order to select the kinetics of only one type of optical centers.

The crystalline beta phase of bulk TCP is characterized by a large unit cell. As shown in [51], its unit cell contains a huge number of atomic positions obeying the noncentrosymmetric space group R3c. Previous studies have also shown the presence of a large number of stoichiometric substitutions in bulk $\text{Ca}_3(\text{PO}_4)_2$ [52–56]. However, it remains unclear how the local geometry and bond distances change during cation exchange and to what extent these changes affect material properties. Moreover, if we take into account the peculiarities of chemical synthesis, knowledge about the possible effect of trapped hydroxyl groups on the distribution of trivalent impurities in the crystal lattice is of particular interest. We chose the Nd^{3+} ion as a luminescent probe to track changes in the local crystal structure, since absorption and fluorescence spectral lines of Nd^{3+} are located in the so-called “first” biological window (700–1000 nm). This makes it possible to detect the Nd^{3+} ion fluorescence not only on the surface of the tissue, but also at a depth of up to one centimeter. On the other hand, information about various geometry parameters, constraints and local distortions can be predicted using quantum chemical calculations.

In this part of the work, we investigated the distribution of Nd^{3+} impurity optical centers over five Ca^{2+} positions in the $\beta\text{-Ca}_3(\text{PO}_4)_2$ lattice (space group R3c) using low-temperature laser site-selective spectroscopy and analysis of the fluorescence kinetics measured by double spectral selection in combination with the results of calculations of periodic density functional theory (DFT).

5.3.1. Computational part

Computational work was performed using the Vienna ab initio simulation package (VASP) [57, 58] together with the potential projector augmented-wave (PAW) method [59, 60]. Geometry relaxation and ground state equilibrium studies were performed within the density functional theory (DFT) method using the Perdew-Burke-Ernzerhof (PBE) functional generalized gradient approximation (GGA) [61]. The calculations employed the plane-wave basis and PAW-PBE pseudopotentials, which corresponded to $5s^25p^64f^46s^2$, $3s^23p^64s^23d^0$, $3s^23p^3$ и $2s^22p^45s^25p^64f^46s^2$, $3s^23p^64s^23d^0$, $3s^23p^3$ and $2s^22p^4$ valence electrons configurations for Nd, Ca, P, and O, respectively. To calculate the electronic structure, a plane wave energy cutoff of 500 eV was used together with Gamma-centered $2 \times 2 \times 1$ k-points set for integration over Brillouin zone. All calculations were spin-polarized. The Nd^{3+} inclusion was modeled in a standard β - $Ca_3(PO_4)_2$ unit cell with the assumption that Nd^{3+} can be located at the lattice site that occupies the Ca^{2+} cation in the undoped lattice.

The main assumption was made that in the beta modification of calcium triphosphate doped with Nd^{3+} ions, optical centers are formed upon heterovalent substitution of Nd^{3+} ions for Ca^{2+} ions. In this case, two different mechanisms for compensating the excess charge are possible: with the help of molecular OH^- groups present in the structure due to the water synthesis method, or when three Ca^{2+} ions are replaced by two Nd^{3+} ions and a vacancy.

First, we modeled the structural behavior of a single water molecule intercalated into a β -TCP unit cell. Based on the DFT simulation, we investigated if there are empty spaces in the lattice that could provide the preferred placement of the water molecule.

We found that the empty spaces, into which the water molecule should intercalate, belong only to one-dimensional channels, which are formed by vertical chains of "widely spaced" Ca4 or Ca5 cations. Our calculations showed that a single H_2O molecule relatively easily occupies these positions, since no noticeable structural distortions of the local environment are observed. Moreover, the packaging efficiency can be confirmed by the fact that the volumetric strain associated with intercalation appears to be small ($\max|\Delta V/V| < 0,65\%$). This means that when water is embedded in the β -TCP trigonal lattice, it prefers to occupy a position in which it does not interact strongly with neighboring ions that form its local crystalline environment. In other words, when we consider the possible configurations of water molecules in the lattice space, we assume a flexible model of their distribution in terms of their coordination with the nearest neighbors.

As a result of calculations, it was shown that the formation of various types of $Nd^{3+} - OH^-$ optical centers is possible in the crystal lattice of Nd^{3+} : β -TCP. For four optical centers of this type with the highest defect formation energy, the distances between the ion and the nearest OH-molecule were calculated (Table 3).

Table 4. Graphical representation of Nd³⁺ coordinations for the model system Nd₂₆Ca₁₀(PO₄)₇. The cation is shown with a green (Ca²⁺) or purple (Nd³⁺) ball, coordinated oxygen ions with red balls. The cation-oxygen distances are indicated in Å. Abbreviation ‘w/o Ca...’, etc. means a vacant lattice site created at a given crystallographic position.

Nd(Ca3)–Nd(Ca3) (w/o Ca4) (4.37 Å; 0.90 eV)	Nd(Ca2)–Nd(Ca3) (w/o Ca4) (7.56 Å; 1.13 eV)	Nd(Ca1)–Nd(Ca3) (w/o Ca4) (7.39 Å; 1.14 eV)
Nd(Ca2)–Nd(Ca2) (w/o Ca4) (4.60 Å; 1.24 eV)	Nd(Ca2)–Nd(Ca3) (w/o Ca4) (3.82 Å; 1.34 eV)	Nd(Ca1)–Nd(Ca1) (w/o Ca4) (4.40 Å; 1.39 eV)
Nd(Ca3)–Nd(Ca5) (w/o Ca4) (5.38 Å; 1.92 eV)	Nd(Ca2)–Nd(Ca5) (w/o Ca4) (3.92 Å; 2.03 eV)	Nd(Ca3)–Nd(Ca3) (w/o Ca3) (4.16 Å; 2.25 eV)
Nd(Ca5)–Nd(Ca5) (w/o Ca4) (8.75 Å; 2.77 eV)	Nd(Ca2)–Nd(Ca3) (w/o Ca5) (6.78 Å; 2.79 eV)	Nd(Ca1)–Nd(Ca1) (w/o Ca1) (4.38 Å; 2.86 eV)

Analysis of the results of modeling by the DFT method revealed the following structural features associated with substitution:

- As follows from Tables 3 and 4, doping with Nd^{3+} does not change the point symmetry of the occupied positions. Here we want to emphasize the ability of trigonal symmetry to completely control the geometry of the host lattice. With regard to local distortion, this is due to two key factors. First, this is due to peculiarities of the $R3c$ polar group, which decomposes the cell of the periodic structure only into two different Wyckoff positions – 6a with three-fold symmetry and 18b with a trivial 2π rotation. Thus, no other crystallographic positions are allowed. Secondly, the conventional unit cell is very large compared to the existing interatomic distances; its linear dimensions are much larger than the characteristic lengths of the valence electrons density distribution. Consequently, the introduction of a low concentration of impurities cannot cause spontaneous breaking of point or spatial symmetry.
- Note, that the $\text{Nd}/(\text{Ca}+\text{Nd})$ ratio in synthesized samples does not exceed the value of 1 at. %. Therefore, the spatial arrangement of the intercalated Nd^{3+} ions should be considered in the diluted mode. This means that we can divide defect sites in the β -phase of TCP into two generalized configurations, which differs in the charge-balancing mechanism. The first configuration includes one Nd^{3+} ion, which replaces one of the Ca1, Ca3, or Ca2 ions in position 18b, and the excess charge is compensated using the nearest hydroxyl anion either directly or through the Ca^{2+} cation. The second configuration relates to the case of a Nd^{3+} pair, which is distributed over two calcium sites with a specific geometry shown in the figures in Table 4.

5.3.2. Laser site-selective and kinetic spectroscopy of the Nd^{3+} : β -TCP microceramics

Calculations have shown that in the structure of β -TCP the replacement of Ca^{2+} ions by Nd^{3+} ions can occur in different crystallographic positions, which leads to different local geometries and charge compensation schemes. We tried to find out what Ca^{2+} positions are occupied by the Nd^{3+} ion in this crystal matrix and what is the local structure of the resulting optical centers. For this, the fluorescence excitation spectrum of 0.1 at. % Nd^{3+} : β -TCP was recorded at $T = 4.2$ K in the spectral range of 870–880 nm by scanning a tunable laser in the wavelength range of the $^4\text{I}_{9/2} (1) \rightarrow ^4\text{G}_{5/2} (1,2)$ optical transition of the Nd^{3+} ion (Fig. 16).

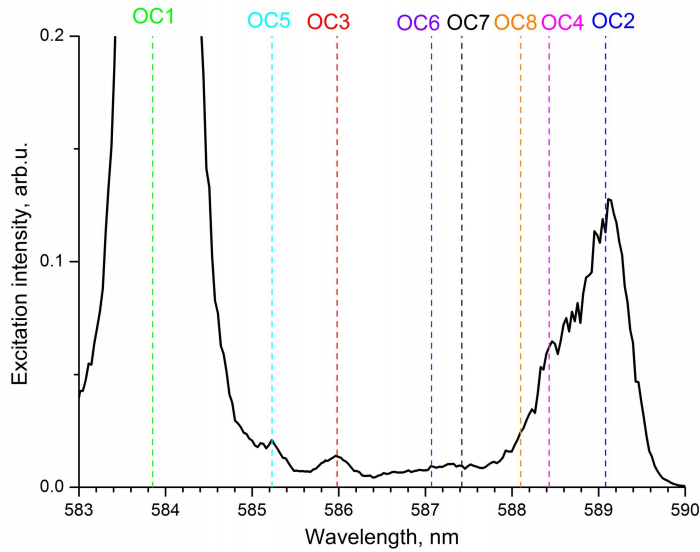


Fig. 16. Fluorescence excitation spectrum of 0.1 at. % Nd^{3+} : β -TCP at $T = 4.2$ K, detected in the spectral range 870–880 nm by scanning a tunable laser in the wavelength range of the $^4\text{I}_{9/2}(1) \rightarrow ^4\text{G}_{5/2}(1,2)$ optical transitions of the Nd^{3+} ion. The dashed lines indicate the excitation wavelengths for selected eight OCs of Nd^{3+} .

Then, to select the fluorescence spectra of various types of optical centers of Nd^{3+} ions, we selectively excited the fluorescence at the maxima of the spectral lines of the fluorescence excitation spectra and at selected wavelengths within the wings of the inhomogeneously broadened profile of the spectral lines of the fluorescence excitation spectrum, where weak lines of other optical centers could be hidden. As a result, eight optical centers were selected, each with its own spectral maximum of excitation (Fig. 17a) and fluorescence (Fig. 17b) (Table 5).

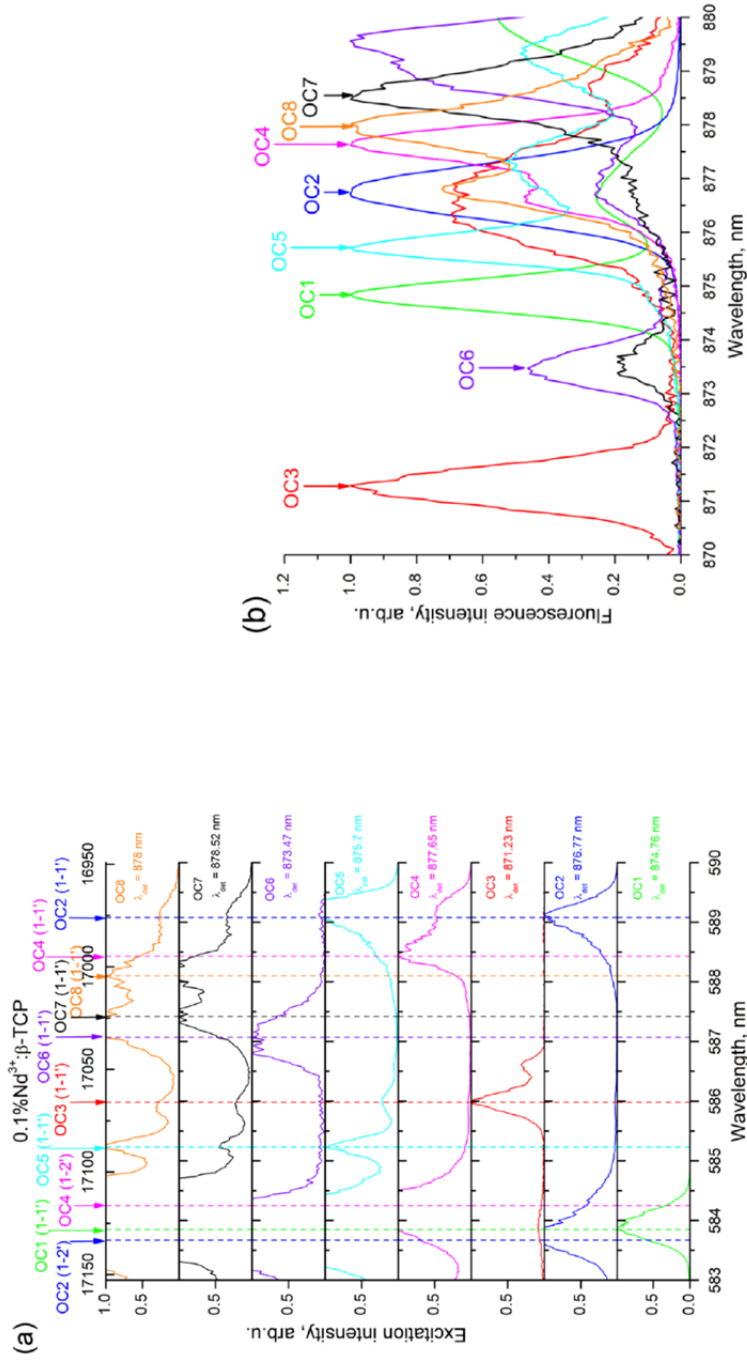


Fig. 17. a) Normalized to their own intensity maxima, site-selective fluorescence excitation spectra of 0.1 at. % Nd^{3+} : β -TCP at $T = 4.2$ K, detected in the maxima of their fluorescence spectral line by scanning a tunable laser in the wavelength range of the $^4\text{I}_{9/2}(1) \rightarrow ^4\text{G}_{5/2}(1,2)$ optical transitions of the Nd^{3+} ion for all eight OCs of Nd^{3+} . The dashed lines indicate the fluorescence excitation wavelengths for the fluorescence spectra of selected eight OC of Nd^{3+} .
b) Normalized to their own intensity maxima, site-selective fluorescence spectra of 0.1 at. % Nd^{3+} : β -TCP at 4.2 K, measured at the $^4\text{F}_{3/2}(1) \rightarrow ^4\text{I}_{9/2}(1)$ transition for all eight OCs of Nd^{3+} . The arrows show maxima of the fluorescence lines at the $^4\text{F}_{3/2}(1) \rightarrow ^4\text{I}_{9/2}(1)$ transition for each OC of Nd^{3+} in 0.1 at. % Nd^{3+} : β -TCP at $T = 4.2$ K.

Table 5. The maxima of the spectral lines of fluorescence excitation and emission spectra measured at the $^4I_{9/2}(1) \rightarrow ^4G_{5/2}(1)$ and the $^4F_{3/2}(1) \rightarrow ^4I_{9/2}(1)$ transition, respectively, for different types of Nd^{3+} ions optical centers. The order of the optical centers is in accordance with the intensity of their fluorescence excitation spectra.*

	OC1	OC2	OC4	OC8	OC5	OC7	OC3	OC6
Transition	green ¹	blue	pink	orange	cyan	black	red	purple
$^4I_{9/2}(1) \rightarrow ^4G_{5/2}(1)$, λ (nm)	874.76	876.77	877.65	878.00	875.70	878.52	871.23	873.47
$^4F_{3/2}(1) \rightarrow ^4I_{9/2}(1)$, λ (nm)	583.83	589.11	588.43	588.04	585.29	587.42	585.96	587.07

*All optical centers are arranged in the order of their fluorescence intensity taking from the same excitation spectrum normalized to the laser intensity. ¹Line colors in Fig. 17.

Fluorescence decay kinetics of 0.1 at. % Nd^{3+} : β -TCP microcrystals for each type of optical center was measured at the fluorescence line maximum of the $^4F_{3/2}(1) \rightarrow ^4I_{9/2}(1)$ transition of Nd^{3+} ions upon excitation to the maximum of the corresponding spectral line in the excitation spectrum at the $^4I_{9/2}(1) \rightarrow ^4G_{5/2}(1)$ transition (Fig. 18). The kinetics differs for different excitation and detection wavelengths (Fig. 18), which confirms our assumption about eight main types of Nd^{3+} optical centers in the material under study. These eight centers give the main contribution to the near infrared luminescence.

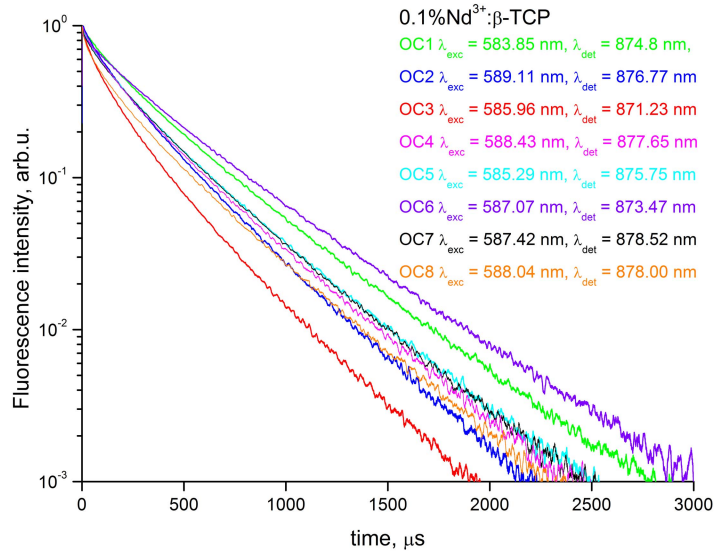


Fig. 18. Luminescence decay kinetics of 0.1 at. % Nd^{3+} : β -TCP at T=4.2 K. In the experiment, the $^4G_{5/2}(1)$ CF level was selectively excited by tunable laser, and the luminescence was selectively detected close to the spectral maximum at the $^4F_{3/2}(1) \rightarrow ^4I_{9/2}(1)$ transition of the corresponding optical center.

Based on the excitation and luminescence spectra, we were able to construct energy diagrams of the $^4G_{5/2}(1)$ and $^4F_{3/2}(1)$ CF (Stark) levels for all eight optical centers (Fig. 19).

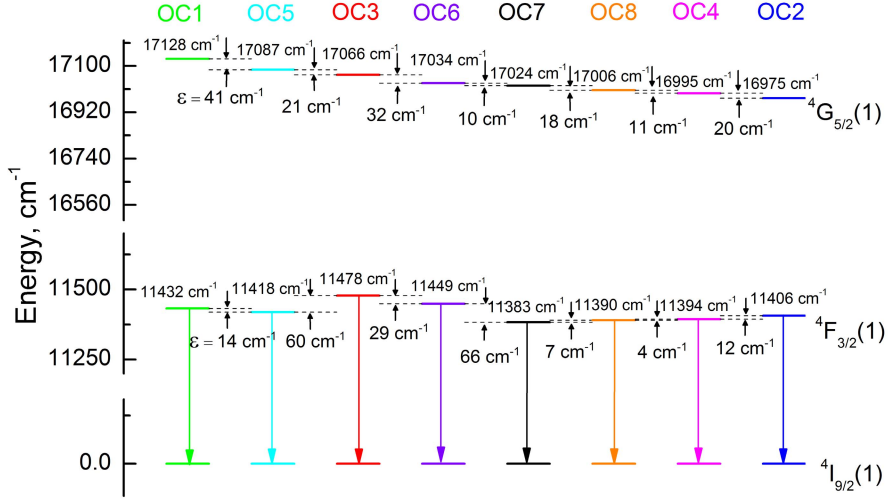


Fig. 19. Energy level diagram of Nd³⁺ ions in the 0.1 at. % Nd³⁺: β-TCP ceramics for eight OCs of Nd³⁺.

An analysis of the concentration luminescence quenching kinetics makes it possible to refine the structure of optical centers, namely, the local environment of an active rare-earth ion. Let us consider the possible processes of fluorescence quenching in our system. The low-energy aqueous synthesis used by us can lead to the formation of a high concentration of crystal structure defects in the volume of the formed nanoparticles [16]. The most significant of these defects are an excess of Nd³⁺-Nd³⁺ pairs and the presence of molecular OH⁻ groups in the crystal structure, which act as acceptors in quenching the NIR luminescence of excited Nd³⁺ ions. In this case, the processes of self-quenching of luminescence (Nd-Nd) and quenching (Nd-OH) can be realized simultaneously [62]. Analysis of the measured FTIR absorption spectra shows the presence of OH⁻ groups in both samples with different concentrations of Nd³⁺ ions (Fig. 20). The spectral peak at 3687 cm⁻¹ appears due to unassociated stretching vibrations of P-OH, which confirms the protonation of phosphate groups. Thus, we have a situation of luminescence quenching on acceptors of two types, which leads to a certain type of impurity quenching kinetics. Namely, at a low concentration of Nd³⁺ (0.1 at. %), an initial exponential ordered stage of static quenching was observed for all eight optical centers (Fig. 21).

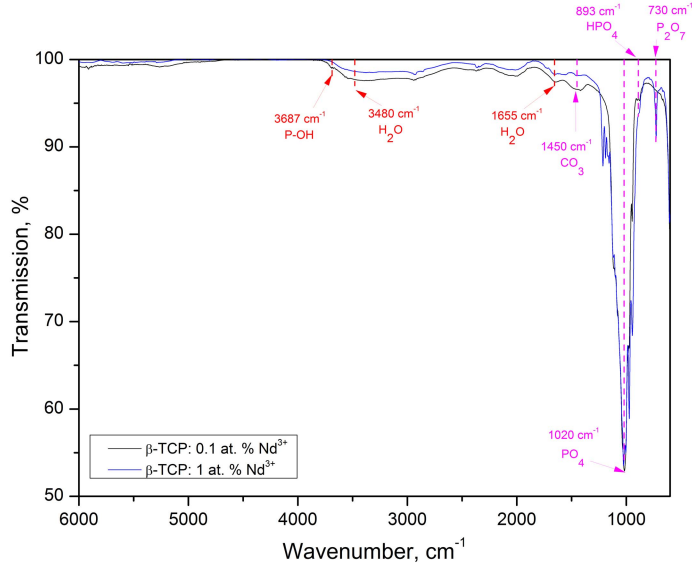


Fig. 20. FTIR absorption spectra of the $\text{Nd}^{3+}:\text{Ca}_3(\text{PO}_4)_2$ powders. Legend is in the figure.

In the simplest case, disregarding the correlation of the two quenching processes, the rate of this stage is additive in terms of the contributions of quenching and self-quenching. For the dipole-dipole interaction between a donor and an acceptor, which is uniquely realized in our case [63], this rate is expressed as [19]

$$W_{ord} = c_{Nd} C_{DA} \sum_{jCa} \frac{1}{R_{ij}^6} + c_{OH} C_{DOH} \sum_{jOH} \frac{1}{R_{ij}^6}, \quad (26)$$

where $c_{Nd} = n_{Nd} / n_{\max}$ and $c_{OH} = n_{OH} / n_{\max}$; $\sum_{jCa} R_{ij}^{-6}$ is the lattice

sum over the Ca^{2+} positions and $\sum_{jOH} R_{ij}^{-6}$ is the lattice sum over the positions around the Nd^{3+} ion, where OH^- groups are embedded during synthesis.

With a uniform distribution of impurity Nd^{3+} ions and OH^- groups over the positions of the crystal lattice, the kinetics of impurity fluorescence quenching at short times after the end of the ordered static stage in the limit of hopping Nd - Nd migration ($C_{DD} \gg C_{DA}$) can be represented as the product of the Förster functions for quenching and self-quenching [62], that is, the decrease in kinetics becomes non-exponential. This may be followed by a short exponential stage of migration-accelerated quenching with a transition to a non-exponential, similar to the Förster fluctuation asymptotics [17].

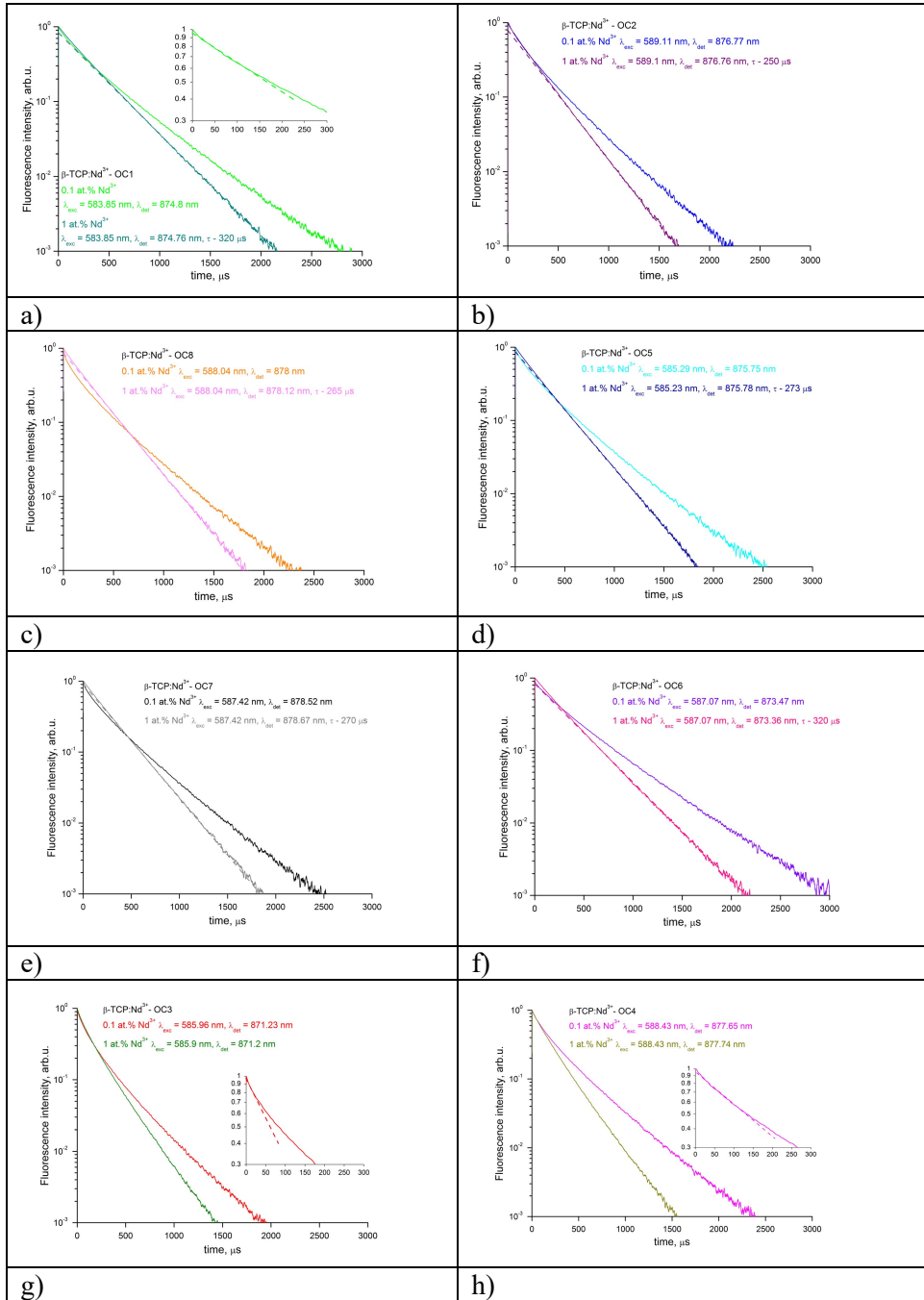


Fig. 21. Fluorescence kinetics of 0.1 and 1 at. % Nd³⁺: β -TCP at T=4.2 K for each type of eight optical centers. In the experiment, the $^4G_{5/2}(1)$ CF level was selectively excited by pulsed tunable laser, and the luminescence was selectively detected close to the luminescence spectral maximum at the $^4F_{3/2}(1) \rightarrow ^4I_{9/2}(1)$ transition. Insets are expanded time scale.

An increase in the Nd^{3+} ions concentration up to 1 at. % leads to a change in the fluorescence kinetics for all studied optical centers. The fluorescence kinetics of six optical centers exponentially decays to a depth of three orders of magnitude from the initial luminescence intensity (Fig. 21, a–f). Such a decay with an increase in the neodymium ions concentration usually indicates an ordered static decay associated with Nd-Nd self-quenching. In case of a random distribution of neodymium ions over the positions of the lattice cations, this is usually observed in the entire time range of the kinetics of luminescence quenching only at very high dopant concentrations [41]. However, since the concentration of neodymium ions is rather low, only 1 at. %, then we can talk about the formation of isolated pairs of Nd^{3+} ions, similar to pair M-centers in the Nd^{3+} : CaF_2 crystal, where, due to the heterovalent substitution of Ca^{2+} by Nd^{3+} , exponentially decaying fluorescence kinetics of the $^4\text{F}_{3/2}$ (1) level of Nd^{3+} ion is observed even at an impurity concentration of 0.6 at. % [64]. In the Nd^{3+} : β -TCP crystal, the formation of such pairs is energetically favorable to compensate for the excess charge of the neodymium ion according to the $3\text{Ca}^{2+} \rightarrow 2\text{Nd}^{3+} + \square$ scheme.

5.3.3. Determination of the structure of the local environment of optical centers in Nd^{3+} : β -TCP microceramics

DFT calculations performed for a concentration of Nd^{3+} ions close to 1 at. % show the formation of a large number of Nd^{3+} - Nd^{3+} pairs in the Nd^{3+} : β -TCP crystal (Table 3), while the number of such pairs at a concentration of 0.1 at. % Nd^{3+} , when calculation is difficult, should be much less. Instead of Nd^{3+} - Nd^{3+} pairs, the formation of Nd^{3+} - OH^- pairs is possible when the charge is compensated by OH^- ions located close to the Nd^{3+} ion. In this respect, the behavior of the luminescence quenching kinetics at a given concentration of Nd^{3+} ions will be similar to that, for example, for nanocrystals of 0.1 at. % Nd^{3+} : YPO_4 , where OH^- groups are present in the crystal structure due to protonation of the $(\text{PO}_4)^{3-}$ groups during aqueous synthesis, despite the homovalent substitution of Y^{3+} by Nd^{3+} , when charge compensation is not required [9]. In this case, the luminescence kinetics has a short initial exponential stage due to quenching at the nearest acceptors. The rest of the kinetics is a non-exponentially decaying curve described by the Förster equation for static disordered quenching by randomly distributed acceptors located at a distance $R \gg R_{\min}$ from the excited donor.

Among the detected optical centers, two of them, namely the optical centers OC3 and OC4, have a luminescence kinetics that remains non-exponential at a late stage at 1 at. % Nd^{3+} , but with deeper quenching than at 0.1 at. % Nd^{3+} (Fig. 21; g, h). Such kinetics can be observed only in the absence of Nd^{3+} pairs, i.e. in the case of single optical centers of the Nd^{3+} ion. According to the calculated data, several types of Nd-OH optical centers can be formed in Nd^{3+} : β -TCP.

The defect formation energy for a particular optical center will directly affect the number of these optical centers in the material, and hence the absolute intensity of their luminescence. However, in this case, one should also take into account the probability of spontaneous radiative decay, which is inversely proportional to the lifetime of the optical center. The longer the lifetime is, and hence the lower the probability of spontaneous radiative decay is, the less intense the fluorescence of the optical center will be. Also, important information is provided by the lifetime for pair Nd^{3+} - Nd^{3+} optical centers at a concentration of 1 at. % Nd^{3+} . It can be assumed that the shorter the kinetics for a particular optical center is the shorter the distance in a pair of neodymium ions will be since the rate of luminescence quenching is inversely proportional to the sixth power of the distance between the donor and acceptor (expression 26).

It is known [19] that the larger the minimum distance to the neighboring acceptor is, the less the fluorescence quenching will be and the longer the stage of ordered static quenching will be. However, when analyzing the initial stage of the impurity quenching kinetics, it is also necessary to take into account the spectral energy migration to optical centers with lower energy levels. According to the energy level diagram (Fig. 19), the Stark level ${}^4\text{F}_{3/2}(1)$ of the OC3 optical center lies above the levels of the other OCs, and therefore nonradiative spectral energy migration from it to other types of optical centers of the Nd^{3+} ion, accompanied by the emission of one phonon, is possible. In the low-temperature limit, its rate is proportional to the mismatch of the energy resonance ϵ between the levels of the donor and acceptor and, therefore, is most effective between optical centers with the largest energy mismatch [65]. Thus, the spectral migration from OC3 over the ${}^4\text{F}_{3/2}(1)$ C.F. level most likely can take place to OC2 ($\epsilon = 72 \text{ cm}^{-1}$), OC4 ($\epsilon = 84 \text{ cm}^{-1}$), OC7 ($\epsilon = 95 \text{ cm}^{-1}$) and OC8 ($\epsilon = 88 \text{ cm}^{-1}$). We have confirmed the presence of spectral migration from OC3 to OC2 and OC4. Spectral migration from OC3 to OC7 and OC8 was not observed because of the low concentration of optical centers OC8 (large average distance between OC3 and OC8). In the case of OC7 this is due to the large minimum distance between OC3 and OC7.

Thus, in order to compare the calculated and experimental results and determine the local crystal field structure for each of experimentally detected optical centers, we used the following calculated and experimental data. From calculations by the DFT method, we used the type of charge compensation for heterovalent substitution of Ca^{2+} for Nd^{3+} ions, the defect formation energy for each configuration, as well as the distance to the nearest acceptor, neodymium ion for paired centers or OH^- for single optical centers. The addition of experimental data made it possible to identify these centers based on the values of the relative luminescence intensity for different types of OCs (Table 6) and by the temporal profile of their luminescence decay kinetics (Fig. 21). As a result, it was possible to determine the configurations of eight types of Nd^{3+} optical centers, which make the main contribution to the NIR fluorescence of β -TCP (Table 6).

Table 6. Comparison of calculated and experimental data on the replacement of ions Ca^{2+} by Nd^{3+} ions in β -TCP micropowders.

OC №	0.1% Nd^{3+} , intensity, counts	1% Nd^{3+} , intensity, counts	τ (1 at. % Nd^{3+}), μs	Ordered stage	$R_{\text{Nd-Nd}}/R_{\text{Nd-OH}}$, Å	ΔW , eV	Center configuration
1	185757	250000	320	Yes	7.56/-	1.13	Nd(Ca2) – Nd(Ca3)
					7.39/-	1.14	Nd(Ca1) – Nd(Ca3)
2	44000	50000	250	Yes	4.37/-	0.90	Nd(Ca3) – Nd(Ca3)
4	19000	28000	245	No	-/2.40	1.08	Nd(Ca3) – OH
8	3950	7400	265	Yes	3.82/-	1.34	Nd(Ca2) – Nd(Ca3)
5	3450	21100	273	Yes	5.38/	1.92	Nd(Ca3) – Nd(Ca5)
7	2400	5600	270	Yes	4.38/-	1.39	Nd(Ca1) – Nd(Ca1)
3	2250	5480	232	No	-/2.34	0.98	Nd(Ca1) – OH
6	712	3450	320	Yes	3.92/-	2.03	Nd(Ca2) – Nd(Ca5)

Special attention should be paid to the optical center OC1. DFT calculations showed that the lowest defect formation energy is observed for the Nd(Ca3)-Nd(Ca3) configuration (0.90 eV) (Table 4). However, in this configuration the distance between Ca^{2+} ions is small (4.366 Å). Consequently, the optical center of this configuration cannot have the most intense luminescence and a long fluorescence decay time, as is observed for OC1, due to strong fluorescence self-quenching. The next configurations in terms of the defect formation energy are Nd(Ca1) – Nd(Ca3) and Nd(Ca2) – Nd(Ca3). Taking into account that OC1 fluorescence is about five times more intense than the next largest OC2 fluorescence, we assumed that OC1 luminescence is the sum of luminescence of two optical centers with the calculated Nd (Ca1) – Nd (Ca3) and Nd (Ca2) – Nd (Ca3) configurations. These two configurations are very similar and therefore are weakly spectrally separated. They have a large distance between neodymium ions in a pair of 7.56 Å and 7.39 Å, respectively. Therefore, the luminescence of these optical centers is weakly quenched by cross-relaxation (Table 4).

SUMMARY

The main goal of the thesis was to study the radiative and nonradiative relaxation of optical excitation energy in crystalline matrices of various scales, such as bulk crystals, microceramics and nanoparticles, using laser site-selective and kinetic spectroscopy. The following main results were obtained:

1. New experimental data on the concentration dependence of the fluorescence kinetics in a bulk $\text{Nd}^{3+}:\text{LaF}_3$ crystal were consistently described using a single set of microparameters for energy migration C_{DD} and cross-relaxation energy transfer C_{DA} .
2. An investigation was made of the concentration dependence of impurity luminescence for aqueous colloidal solutions of $\text{Nd}^{3+}:\text{LaF}_3$ and $\text{Nd}^{3+}:\text{KY}_3\text{F}_{10}$ nanoparticles, including the fluorescence kinetics, its relative fluorescence quantum yield associated only with inter-center fluorescence quenching, and fluorescence brightness as the product of its relative quantum yield and the concentration of impurity ions. For each crystal matrix, the optimal impurity concentration was determined for the maximal brightness of the NIR fluorescence.
3. Simple criteria were established for choosing a crystal matrix for doping with Nd^{3+} ions in the synthesis of aqueous colloidal solutions of nanocrystals to use them as luminescent probes in the “first biological window” (750–950 nm), which is most convenient for luminescence recording. This is a large ratio of intensity parameters Ω_4/Ω_6 , used in the Judd-Ofelt theory to calculate the probability of radiative transitions. This increases the fluorescence branching ratio β at the $^4\text{F}_{3/2} \rightarrow ^4\text{I}_{9/2}$ transition lying in the “first biological window”. The second one is a low value of the intensity parameter Ω_6 that reduces the strength of the ion-ion interaction and makes Nd-Nd self-quenching and Nd-OH⁻ quenching weaker.
4. The analysis of fluorescence quenching in the near-IR spectral range in neodymium-doped $\beta\text{-Ca}_3(\text{PO}_4)_2$ microceramics with heterovalent substitution of Nd^{3+} ions for Ca^{2+} ions has been carried out. Laser site-selective and kinetic spectroscopy have shown the difference in the fluorescence quenching of various types of optical centers and established the reasons for this difference associated with the appearance of two kinds of optical centers: pairs of neodymium ions (Nd-Nd) with a small distance between ions and therefore strongly quenched fluorescence, and the Nd-OH closely spaced ions, where the OH⁻ ion acts as an acceptor quenching the fluorescence of the associated Nd^{3+} ion. These OH⁻ molecular groups are embedded in the structure of the crystal lattice during aqueous synthesis.
5. Combining the methods of laser site-selective and kinetic spectroscopy, as well as the results of quantum chemical calculations (DFT), it was possible to determine the type and local crystal field symmetry of eight types of Nd^{3+} optical centers, which make the main contribution to the NIR luminescence.

Six optical centers turned out to be pair Nd^{3+} - Nd^{3+} optical centers formed even at a low impurity concentration due to the heterovalent substitution of Nd^{3+} for Ca^{2+} ions according to the scheme $3\text{Ca}^{2+} \rightarrow 2\text{Nd}^{3+} + \square$, where one calcium position remains vacant. Two optical centers are single centers of the Nd^{3+} ions in which the charge is compensated by negatively charged ions of OH^- molecular groups intercalated during hydrothermal synthesis according to the $2\text{Ca}^{2+} \rightarrow \text{Nd}^{3+} + \text{OH}^-$ scheme.

SUMMARY IN ESTONIAN

Fluorestsentsi kustutamine neodüümi ionidega aktiveeritud anorgaanilistes tahkistes, mahumaterjalidest mikro- ja nanokristallideni.

Väitekirja põhieesmärk oli optilise ergastusenergia kiirgusliku ja mittekiirgusliku relaksatsiooni uurimine kristallilises maatriksis erinevates mastaapides, sh mahumaterjalides, mikrokeraamikas ja nano-osakestes, kasutades kohtselektiivset ja aeglahutusega laserspektroskoopiat. Põhitulemused on järgmised:

1. Uued eksperimentaalsed andmed Nd^{3+} : LaF_3 mahukristalli fluorestsentsi kineetika kontsentratsioonisõltuvuse kohta õnnestus kooskõlaliselt kirjeldada ühe komplekti energiaülekande mikroparameetritega energia migratsiooni (C_{DD}) ja ristrelaksatsiooni (C_{DA}) jaoks.
2. Uuriti Nd^{3+} : LaF_3 ja Nd^{3+} : KY_3F_{10} nanoosakeste lisandifluorestsentsi kolloidsetes vesilahustes, sh fluorestsentsi kineetikat, tsentritevahelise kustutamise seotud suhtelist kvantsaagist, ja fluorestsentsi heledust kui suhtelise kvantsaagise ja lisandioonide kontsentratsiooni korrutist. Iga kristalli jaoks tehti kindlaks optimaalne lisandi kontsentratsioon, mis maksimeeris vaadeldava lähi-infrapunase fluorestsentsi heleduse.
3. Formuleeriti lihtsad kriteeriumid kristallmaatriksi valimiseks Nd^{3+} lisandioonidele nanokristallides, mis sünteesitakse kolloidses vesilahuses kasutamiseks fluorestsents-märgistena bioloogilise koe läbipaistvusalas 750–950 nm, kus luminesentsi registreerimine on kõige mugavam. Selleks peab, ühelt poolt, Judd-Ofelti teoorias kiirguslike siirete tõenäosuse arvutamiseks kasutatavate intensiivsuspameetrite suhe Ω_4/Ω_6 olema suur. See suurendab fluorestsentsi tõenäosust (hargnemissuhet β) ülemineku $^4\text{F}_{3/2} \rightarrow ^4\text{I}_{9/2}$ jaoks, mis asub nimetatud bioloogilises läbipaistvusaknas. Teiselt poolt, intensiivsuspameetri Ω_6 väärtus peaks olema väike, sest see vähendab ionidevahelist interaktsiooni ja seeläbi fluorestsentsi kustutamist nii teiste Nd ionide (Nd-Nd isekustutamine) kui ka OH^- rühmade poolt.
4. Analüüsiti fluorestsentsi kustutamist lähi-infrapunases piirkonnas neodüümi-ga dopeeritud $\beta\text{-Ca}_3(\text{PO}_4)_2$ mikrokeraamikas, kus osa Ca^{2+} ioone on heterovalentselt asendatud Nd^{3+} lisandioonidega. Koht-selektiivne aeglahutusega spektroskoopia näitas, et mitmesuguste optiliste tsentrite fluorestsents on kustutatud erineval määral, ja võimaldas kindlaks teha selle põhjused, mis on seotud kahte eri tüüpi optiliste tsentrite esinemisega. Ühel juhul on optilise tsentri koosseisus lähedikkude paiknevate neodüümi ionide paar (Nd-Nd), mille fluorestsents on seega tugevasti kustutatud. Teisel juhul moodustab optilise tsentri üksus Nd-OH, kus OH rühm toimib aktseptorina, mis kustutab seotud Nd^{3+} iooni fluorestsentsi. Need OH^- rühmad sisenevad kristallstruktuuri vesilahusest sünteesimise käigus.

5. Koht-selektiivse aeglahutusega laserspektroskoopia ja kvantkeemiliste arvutuste (DFT) kombineerimisel osutus võimalikuks tuvastada kaheksa põhilist Nd^{3+} optilist tsentrit (mis panustavad lähi-infrapunasesse kiirgusse) ja määrata nende lokaalne kristallivälja sümmeetria. Neist kuus optilist tsentrit moodustuvad Nd^{3+} - Nd^{3+} ioonpaaridest. Nende tekkimine leiab aset isegi väikesel lisandi kontsentratsioonidel tingituna Ca^{2+} heterovalentselt asendusest Nd^{3+} ionidega vastavalt skeemile $3\text{Ca}^{2+} \rightarrow 2\text{Nd}^{3+} + \square$, kus üks kaltsiumi positsioon jääb vakantseks. Seevastu kaks ülejäänud optilist tsentrit sisaldavad vaid ühe Nd^{3+} iooni, kus laeng on kompenseeritud OH^- molekulaarrühmadega ($2\text{Ca}^{2+} \rightarrow \text{Nd}^{3+} + \text{OH}^-$), mis sisenevad kristalli koosseisu hüdrotermilise sünteesi käigus.

ACKNOWLEDGEMENTS

I am very grateful to my supervisors Yu.V. Orlovskiy, V. Kiisk and V. Peet for support and guidance. Also, I am thankful to all colleagues from the laboratories of Laser Spectroscopy, Institute of Physics and Laser Spectroscopy of Solid State, A.M. Prokhorov General Physics Institute RAS, and especially L. Puust, L. Dolgov, and A.V. Popov for their assistant with experimental work and S.Kh. Batygov, E.O. Orlovskaya, and A.S. Vanetsev for the synthesis of the fluoride crystals and nanocrystals. Special thanks to M. Janulevičius for help in the synthesis of beta-tricalcium phosphate microceramics.

I acknowledge Russian Science Foundation (grant RSF 16-02-10077) and Estonian Research Council (grant PRG347) for financial support.

REFERENCES

1. H. Oonishi, Orthopedic Applications of Hydroxyapatite, *Biomaterials*, Vol 12, 1991, p 171–178
2. Triglia J. M., Scheiner C., Gouvernet J., Cannoni M., Hydroxyapatite in Experimental Laryngotracheal Reconstruction, *Achieves of otolaryngology – head & neck surgery*, 119 (1), 1993, 87–91.
3. Wang F., Banerjee D., Liu Y., Chen X., Liu X., Upconversion nanoparticles in biological labeling, imaging, and therapy, *Analyst*, 135–8, 2010, 1839–1854.
4. Wang K., Ma J, He M., Gao G., Xu H., Sang J., Wang Y, Zhao B, Cui D., Toxicity Assessments of Near-infrared Upconversion Luminescent LaF₃: Yb, Er in Early Development of Zebrafish Embryos; *Theranostics*, 3–4, 2013, 258–266
5. Di W., Shirahata N., Zeng H., Sakka Y., Fluorescent sensing of colloidal CePO₄: Tb nanorods for rapid, ultrasensitive and selective detection of vitamin C, *Nanotechnology*, 21, 2010, 365501
6. Lv R., Yang G., He F., Dai Y, Gai S, Yang P, LaF₃: Ln mesoporous spheres: controllable synthesis, tunable luminescence and application for dual-modal chemo-/photo-thermal therapy, *Nanoscale*, 6, 2014, 14799–14809.
7. Cheng S., Liu L., Yang QH., Li Y., Zeng S., In vivo optical bioimaging by using Nd-doped LaF₃ luminescent nanorods in the second near-infrared window, *Journal of Rare Earths*, 37, 2019, 931–936.
8. Rocha U., Hu J., Rodríguez E. M., Vanetsev A. S., Rähn M., Sammelselg V., Orlovskii Yu. V., Solé J. G., Jaque D., Ortgies D. H., Subtissue imaging and thermal monitoring of gold nanorods through joined encapsulation with Nd-doped infrared-emitting nanoparticles, *Small*, 12 (39), 2016, 5394–5400.
9. Samsonova E., Popov A. V., Vanetsev A. S., Keevend K., Orlovskaya E. O., Kiisk V., Lange S., Joost U., Kaldvee K., Maeorg U., Glushkov N. A., Ryabova A. V., Sildos I., Osiko V. V., Steiner R., Loschenov V. B., Orlovskii Y. V., An energy transfer kinetic probe for OH-quenchers in the Nd³⁺: YPO₄ nanocrystals suitable for imaging in the biological tissue transparency window, *Physical Chemistry Chemical Physics*, 16, 2014, 26806–26815.
10. K. Kaldvee, A.V. Nefedova, S.G. Fedorenko, A.S. Vanetsev, E.O. Orlovskaya, L.Puust, M. Pärss, I.Sildos, A.V.Ryabova, Yu.V.Orlovskii, Approaches to contactless optical thermometer in the NIR spectral range based on Nd³⁺ doped crystalline nanoparticles, *J. of Lumin.*, 183 (2017) 478–485.
11. Johnsson N., Johnsson K., Chemical Tools for Biomolecular Imaging, *ACS Chemical Biology*, 1, 2007, 31–38.
12. Prasad G.L., Biomedical Applications of Nanoparticles, in: *Safety of Nanoparticles (From Manufacturing to Medical Applications)*, Ed. Thomas J. Webster, Springer, 2009, 89–109.
13. Gnach A., Lipniski T., Bednarkiewicz A., Rybka J., Capobianco J. A., Upconverting nanoparticles: assessing the toxicity, *Chemical Society Review*, 44, 2015, 1561–1584.
14. Longmire M., Choyke P.L., Kobayashi H., Clearance properties of nano-sized particles and molecules as imaging agents: considerations and caveats, *Nano-medicine* 3, 5, 2008, 703–717.
15. Vanetsev A.S., Samsonova E.V., Gaitko O.M., Keevend K., Popov A.V., Mäeorg U., Mändar H., Sildos I., Orlovskii Yu.V., Phase composition and morphology of nanoparticles of yttrium orthophosphates synthesized by microwavehydrothermal

- treatment: the influence of synthetic conditions, *J. Alloys Compd.*, 639, 2015, 415–421.
16. Vanetsev A., Kaldvee K., Puust L., Keepend K., Nefedova A., Fedorenko S., Baranchikov A., Sildos I., Rahn M., Sammelselg V., Orlovskii Yu., Relation of Crystallinity and Fluorescent Properties of $\text{LaF}_3\text{:Nd}^{3+}$ Nanoparticles Synthesized with Different Water-Based Techniques, *ChemistrySelect*, V. 2, 2017, 4874–4881.
 17. Orlovskii Yu. V., Popov A.V., Platonov V.V., Fedorenko S.G., Sildos I., Osipov V.V., Fluctuation kinetics of fluorescence hopping quenching in the $\text{Nd}^{3+}\text{:Y}_2\text{O}_3$ spherical nanoparticles, *Journal of Luminescence*, 139, 2013, 91–97.
 18. A. A. Kaminski, Laser Crystals, 2nd ed., *Springer*, (1990), Berlin.
 19. V. P. Sakun, Kinetics of energy transfer in crystals, *Sov. Phys. Solid State*, 14, 1972, 1906–1914.
 20. Förster T., Zwischenmolekulare energiewanderung und fluoreszenz, *Ann. Phys.* 2, 1948, 55–75.
 21. Levitz P., Drake J. M., Klafter J., Critical evaluation of the application of direct energy transfer in probing the morphology of porous solids, *J. Chem. Phys.*, 89, 1988, 5224–5236.
 22. Burshtein A. I., Doktorov A. B., Kiprianov A. A., Morozov V. A., Fedorenko S. G., Regions of applicability of kinematic mechanisms in bimolecular processes, *JETP* 61, 3, 1984, 516–521.
 23. Bodunov E.N., Malyshev V.A., Self-consistent theory of concentration self-quenching, *Opt. Spectrosc.* 62, 1987, 1280–1286 (in Russian).
 24. Sakun V.P., On the kinetic similarity of the processes of concentration quenching and self-quenching of luminescence in disordered activated systems, *Khim. Fiz.*, 6, 1987, 1032–1037 (in Russian).
 25. Gochanour C.R., Andersen H.C., Fayer M.D., Electronic excited state transport in solution, *J. Chem. Phys.*, 70, 1979, 4254–4271.
 26. Loring R.F., Andersen H.C., Fayer M.D., Electronic excited state transport and trapping in solution, *J. Chem. Phys.* 76, 1982, 2015–2027.
 27. Fedorenko S.G., Burshtein A.I., What are the GAF and LAF approaches in essence? *Chem. Phys.*, 98, 1985, 341–349.
 28. Fedorenko S.G., Burshtein A.I., Kipriyanov A.A., Fluctuation asymptotic of hopping quenching in disordered systems, *Phys. Rev. B*, 48, 1993, 7020–7029.
 29. Popov A.V., Orlovskii Yu.V., Vanetsev A.S., Gaitko O.M., Orlovskaya E.O., Sildos I., Nanosecond fluctuation kinetics of luminescence hopping quenching originated from the $5d^1$ level in the $\text{Ce}^{3+}\text{:YPO}_4\cdot 0.8\text{H}_2\text{O}$ nanocrystals, *J. Lumin.*, 145, 2014, 774–778.
 30. Kaminskii A.A., Boulon G., Buoncristiani M., Bartolo B. Di, Kornienko A., Mironov V., Spectroscopy of a new laser garnet $\text{Lu}_3\text{Sc}_2\text{Ga}_3\text{O}_{12}\text{:Nd}^{3+}$. Intensity luminescence characteristics, stimulated emission, and full set of squared reduced-matrix elements $|\langle U(t) \rangle|^2$ for Nd^{3+} ions, *Phys. Status Solidi (a)*, 141 (2), 1994, 471–494.
 31. Burshtein A.I., Hopping mechanism of energy transfer, *Sov. Phys. JETP* 35, 1972, 882–885.
 32. Fedorenko S.G., Burshtein A.I., Binary theory of impurity quenching accelerated by resonant excitation migration in a disordered system, *Chem. Phys.*, 128, 1988, 185–198.
 33. Basiev T.T., Orlovskii Yu.V., Nonradiative energy transfer from high-lying highly quenched multiplets of Nd^{3+} in the LaF_3 laser crystal, *Sov. Phys. JETP*, 69, 1989, 1109–1118.

34. Mansmann Von M., Die kristall strukture von lathantrifluorid. 1965, *Ztschr. Kristallogr. Bd.* **122**, S375–398.
35. Kushida T., Energy transfer and cooperative optical transitions in rare-earth doped inorganic materials. I. Transition probability calculation, *J. Phys. Soc. Jpn.* **34** (1973) 1318–1326.
36. Dexter D.L., A theory of sensitized luminescence in solids, *J. Chem. Phys.*, **21**, 1953 836–850.
37. Meijer J. M., Aarts L., B.M. van der Ende, Vlugt T.J.H., Meijerink A., Down-conversion for solar cells in $\text{YF}_3\text{:Nd}^{3+}$, Yb^{3+} , *Phys. Rev. B*, **81**, 2010, 035107.
38. Ofelt G.S. Intensities of crystal spectra of rare earth ions, *J. Chem. Phys. AIP Publishing*, **37** (3), 1962, 511–520.
39. Judd B.R. Optical absorption intensities of rare-earth ions, *Phys. Rev. APS*, **127** (3), 1962, 750.
40. Ermolaev V.L., Sveshnikova E.B., Bodunov E.N., Inductive-resonant mechanism of nonradiative transitions in ions and molecules in condensed phase, *Phys. Usp.*, **39**, 1996, 261–282.
41. S.G. Fedorenko, A.V. Popov, E.A. Vagapova, A.E. Baranchikov, Yu.V. Orlovskii, Concentration self-quenching of luminescence in crystal matrices activated by Nd^{3+} ions: theory and experiment, *J. Lumin.* **198** (2018) 138–145.
42. T.H. Allik, L.D. Merkle, R.A. Utano, B.H.T. Chai, J.-L.V. Lefausheur, H. Voss, G.J. Dixon, Crystal growth, spectroscopy, and laser performance, of $\text{Nd}^{3+}\text{:KYF}_4$, *J. Opt. Soc. Am. B* **10** (1993) 633–637.
43. L. Gomes, H. Marconi da Silva, M.D. Linhares, R.U. Ichikawa, L.G. Martinez, I.M. Ranieri, Luminescence properties of Yb: Nd: Tm: KY_3F_{10} nanophosphor and thermal treatment effects, *J. Lumin.* **157** (2015) 285–292.
44. C. Li, Y. Guyot, C. Linares, R. Moncorge, M.F. Joubert, Radiative transition probabilities of trivalent rare-earth ions in LiYF_4 , in: *OSA Proceedings on Advanced Solid-State Lasers*, vol. 15, 1993, pp. 91–95.
45. I.R. Martín, Y. Guyot, M.F. Joubert, R.Yu. Abdulsabirov, S.L. Korableva, V.V. Semashko, Stark level structure and oscillator strengths of Nd ion in different fluoride single crystals, *J. Alloys Compd.* **323–324** (2001) 763–767.
46. A.A. Kaminskii, V.S. Mironov, S.N. Bagaev, N.M. Khaidukov, M.F. Joubert, B. Jacquier, G. Boulon, Spectroscopy and laser action of anisotropic singlecentered $\text{LiKYF}:\text{Nd}^{3+}$ crystals grown by the hydrothermal method, *Phys. Stat. Solidi (a)* **145** (1994) 177–195.
47. X. Xue, Z. Duan, T. Suzuki, R.N. Tiwari, M. Yoshimura, Y. Ohishi, Luminescence properties of $\alpha\text{-NaYF}_4\text{:Nd}^{3+}$ nanocrystals dispersed in liquid: local field effect investigation, *J. Phys. Chem. C* **116** (42) (2012) 22545–22551.
48. W.F. Krupke, Optical absorption and fluorescence intensities in several rare-earth doped Y_2O_3 and LaF_3 single crystals, *Phys. Rev.* **145** (1966) 326–336.
49. Orlovskii Yu.V., Vanetsev A.S., Keevend K., Kaldvee K., Samsonova E.V., Puust L., del Rosal B., Jaque D., Ryabova A.V., Baranchikov A.E., Lange S., Sildos I., Kikas J., Loschenov V.B., NIR fluorescence quenching by OH acceptors in the Nd^{3+} doped KY_3F_{10} nanoparticles synthesized by microwavehydrothermal treatment, *J. Alloys Compd.*, **661**, 2016, 312–321
50. Pukhov K. K., Basiev T. T., Orlovskii Yu. V., Spontaneous emission in dielectric nanoparticles, *JETP Letters*, **88** (1), 2008, 12–18.

51. M. Yashima, A. Sakai, T. Kamiyama, A. Hoshikawa, Crystal structure analysis of β -tricalcium phosphate $\text{Ca}_3(\text{PO}_4)_2$ by neutron powder diffraction, *J. Solid State Chem.* 175 (2003) 272–277.
52. D. Deyneko, I.V. Nikiforov, D. Spassky, Y.Y. Dikhtyar, S. Aksenov, S.Y. Stefanovich, B. Lazoryak, B. Luminescence of Eu^{3+} as a probe for determination of the local site symmetry in the β - $\text{Ca}_3(\text{PO}_4)_2$ related structures, *CrystEngComm* 21 (2019) 5235–5242.
53. L.W. Schroeder, B. Dickens, W. Brown, Crystallographic studies of the role of Mg as a stabilizing impurity in β - $\text{Ca}_3(\text{PO}_4)_2$. II. Refinement of Mg-containing β - $\text{Ca}_3(\text{PO}_4)_2$, *J. Solid State Chem.* 22 (1977) 253–262.
54. A. Bessière, R.A. Benhamou, G. Wallez, A. Lecointre, B. Viana, Site occupancy and mechanisms of thermally stimulated luminescence in $\text{Ca}_9\text{Ln}(\text{PO}_4)_7$ (Ln = lanthanide), *Acta Mater.* 60 (2012) 6641–6649.
55. A.E. Khouri, M. Elaattmani, G. Della Ventura, A. Sodo, R. Rizzi, M. Rossi, F. Capitelli, Synthesis, structure refinement and vibrational spectroscopy of new rare-earth tricalcium phosphates $\text{Ca}_9\text{RE}(\text{PO}_4)_7$ (RE = La, Pr, Nd, Eu, Gd, Dy, Tm, Yb), *Ceram. Int.* 43 (2017) 15645–15653.
56. E.S. Zhukovskaya, D. Deyneko, O. Baryshnikova, A. Belik, I. Leonidov, A. Ishchenko, A. S.Y. Stefanovich, V. Morozov, B. Lazoryak, Crystal structure, dielectric, and optical properties of β -calcium orthophosphates heavily doped with ytterbium, *J. Alloy. Compd.* 787 (2019) 1301–1309.
57. G. Kresse, J. Hafner, Ab initio molecular dynamics for liquid metals, *Phys. Rev. B* 47 (1993) 558–561.
58. G. Kresse, J. Furthmüller, Efficient iterative schemes for ab initio total-energy calculations using a plane-wave basis set, *Phys. Rev. B* 54 (1996) 11169–11186.
59. P. E. Blöchl, Projector augmented-wave method, *Phys. Rev. B* 50 (1994) 17953–17979.
60. G. Kresse, D. Joubert, From ultrasoft pseudopotentials to the projector augmented-wave method, *Phys. Rev. B* 59 (1999) 1758–1775.
61. J. P. Perdew, K. Burke, M. Ernzerhof, Generalized gradient approximation made simple, *Phys. Rev. Lett.* 77 (1996) 3865–3868.
62. A.G. Fedorenko, Yu.V. Orlovskii, Concentration quenching and self-quenching of luminescence in disordered solid solutions, 22th International conference “Optics and spectroscopy of condensed matter”, Conference proceedings, p. 93–97, September 18–24, Kuban State University, Krasnodar (2016) ISBN 978-5-9908713-2-8
63. Yu.V. Orlovskii, A.V. Popov, E.O. Orlovskaya, A.S. Vanetsev, E.A. Vagapova, M. Rähn, V. Sammelselg, I. Sildos, A.E. Baranchikov, P.V. Grachev, V.B. Loschenov, A.V. Ryabova, Comparison of concentration dependence of relative fluorescence quantum yield and brightness in first biological window of wavelengths for aqueous colloidal solutions of Nd^{3+} : LaF_3 and Nd^{3+} : KY_3F_{10} nanocrystals synthesized by microwave-hydrothermal treatment, *Journal of Alloys and Compounds* 756 (2018) 182–192.
64. Yu.V. Orlovskii, T.T. Basiev, V.V. Osiko, H. Gross, J. Heber, Fluorescence fine narrowing (FLN) and site-selective fluorescence decay of Nd^{3+} centers in CaF_2 , *J. Luminescence* 82 (1999) 251–258
65. R. Orbach, H.M. Crosswhite, H.W. Moos (Eds.), Phonon side-bands and energy transfer, in *Optical properties of ions in crystals*, InterSci. Publ., N.Y., 1967, pp. 445–455.

PUBLICATIONS

CURRICULUM VITAE

Name: Ekaterina Vagapova
Date of birth: March 12, 1994
Nationality: Russian
Phone number: +37253720748
E-mail: ekaterina.vagapova@ut.ee

Education:

2017 M.Sc. Moscow Power Engineering Institute,
Quantum Electronics, Moscow, Russia
2015 B.Sc. Moscow Power Engineering Institute,
Quantum Electronics, Moscow, Russia
2011 Ostrovetskaya general education school, Ostrovtsy,
Moscow region, Russia

Languages: Russian (native), English (C1), Estonian (B1), French (B1)

Career:

2017 – present Junior Researcher, Prokhorov General Physics Institute,
Moscow, Russia
2017–2018 Assistant, Moscow Power Engineering Institute, Department
of General Physics named after V.A. Fabrikant, Moscow,
Russia

Publications included in the thesis:

1. **E.A. Vagapova**, E. Strugovshchikov, E.O. Orlovskaya, A.S. Vanetsev, L. Dolgov, L. Puust, L.D. Iskhakova, U. Mäeorg, A. Pishtshev, Yu.V. Orlovskii, Combined spectroscopic and DFT studies of local defect structures in beta-tricalcium phosphate doped with Nd(III), Journal of Alloys and Compounds, 877, 2021, 160305
2. S.G. Fedorenko, A.V. Popov, **E.A. Vagapova**, A.E. Baranchikov, Yu.V. Orlovskii, Concentration self-quenching of luminescence in crystal matrices activated by Nd³⁺ ions: theory and experiment, Journal of Luminescence, 198, 2018, 138–145.
3. Yu.V. Orlovskii, A.V. Popov, E.O. Orlovskaya, A.S. Vanetsev, **E.A. Vagapova**, M. Rähn, V. Sammelselg, I. Sildos, A.E. Baranchikov, P.V. Grachev, V.B. Loschenov, A.V. Ryabova, Comparison of concentration dependence of relative fluorescence quantum yield and brightness in first biological window of wavelengths for aqueous colloidal solutions of Nd³⁺: LaF₃ and Nd³⁺: KY₃F₁₀ nanocrystals synthesized by microwave-hydrothermal treatment, Journal of Alloys and Compounds, 756, 2018, 182–192

International conferences presentations related to the PhD thesis

1. **E.A. Vagapova**, A.V. Popov, E.O. Orlovskaya, Z. Stankeviciute, A. Kareiva, A.E. Baranchikov, L.D. Iskhakova, I. Sildos, U. Mäeorg, S.G. Fedorenko, Yu.V. Orlovskii, Kinetics of impurity fluorescence quenching of Nd-doped hydroxyapatite Nd^{3+} : $\text{Ca}_{10}(\text{PO}_4)_6(\text{OH})_2$ powders: Nd^* -Nd self-quenching and Nd^* - OH^- quenching, 24th International conference “Optics and spectroscopy of condensed matter”, Conference proceedings, p. 308 – 318, September 16–22, Kuban State University, Krasnodar (2018), Eds. V.A. Isaev, A.V. Lebedev, 372 pages, ISBN 978-5-6041274-0-7
2. **E.A. Vagapova**, E.O. Orlovskaya, A.V. Popov, L. Puust, A.S. Vanetsev, Z. Stankeviciute, J. Januskevicius, M. Janulevičius, A. Kareiva, Yu.V. Orlovskii, Laser spectroscopy of bi-phasic calcium phosphate powders doped by the Nd^{3+} ions, 7th International Conference “Nanotechnologies and Nanomaterials” NANO-2019, August 27–30, Lviv, Ukraine, Book of Abstracts, p. 288
3. **Vagapova E.A.**, Studies of spectral-kinetical properties of bi-calcium phosphate micropowders, doped by Nd^{3+} ions, for biomedical applications, XVI Russian annual conference of young researchers and graduate students “Physical chemistry and technology of inorganic materials” (with international participation) proceedings of the conference, October 1–4, 2019, Moscow, Russia. IMET RAS, Moscow, Russia: IMET RAS, 179–180.
4. **Vagapova E.A.**, Janulevičius M., Strugovshchikov E., Iskhakova L.D., Vanetsev A.S., Pištšev A., Orlovskii Yu.V. Site-selective laser spectroscopy of Nd^{3+} doped beta-modification of calcium triphosphate. Functional Materials & Nanotechnologies 2020 Online Conference, Virtual Vilnius, Lithuania, 23–26 November, 2020. Book of Abstract, p. 39.

Other publications:

E. Vinogradova, L. Dolgov, V.A. Konyushkin, E.O. Orlovskaya, **E.A. Vagapova**, A. Treshchalov, V. Peet, V. Hizhnyakov, Yu.V. Orlovskii, Fluorescence of Nd^{3+} optical centers close to cubic symmetry in a calcium fluoride crystal co-doped with Na^+ , Journal of Luminescence, 234 (2021) 117988.

ELULOOKIRJELDUS

Nimi: Ekaterina Vagapova
Sünniaeg: 12.03.1994
Kodakondus: Venelane
Telefon: +37253720748
E-post: ekaterina.vagapova@ut.ee

Haridustee:

2017 M.Sc. Moskva energeetikainstituut,
kvant- ja optiline elektroonika, Moskva, Venemaa
2015 B.Sc. Moskva energeetikainstituut,
kvant- ja optiline elektroonika, Moskva, Venemaa
2011 Ostrovetskaya keskkool, Ostrovtsy, Moskva piirkond, Venemaa

Keelteoskus: Vene keel (emakeel), inglase keel (C1), eesti keel (B1), prantsuse keel (B1)

Töökogemus:

2017 – praegu Nooremteadur, Prokhorovi nimeline üldfüüsika instituut,
Moskva, Venemaa
2017–2018 Assistent, Moskva energeetikainstituut, V.A. Fabrikanti
nimeline füüsikaosakon, Moskva, Venemaa

Teeside aluseks olevate publikatsioonide loetelu:

1. **E.A. Vagapova**, E. Strugovshchikov, E.O. Orlovskaya, A.S. Vanetsev, L. Dolgov, L. Puust, L.D. Iskhakova, U. Mäeorg, A. Pishtshev, Yu.V. Orlovskii, Combined spectroscopic and DFT studies of local defect structures in beta-tricalcium phosphate doped with Nd(III), Journal of Alloys and Compounds, 877, 2021, 160305
2. S.G. Fedorenko, A.V. Popov, **E.A. Vagapova**, A.E. Baranchikov, Yu.V. Orlovskii, Concentration self-quenching of luminescence in crystal matrices activated by Nd³⁺ ions: theory and experiment, Journal of Luminescence, 198, 2018, 138–145.
3. Yu.V. Orlovskii, A.V. Popov, E.O. Orlovskaya, A.S. Vanetsev, **E.A. Vagapova**, M. Rähn, V. Sammelselg, I. Sildos, A.E. Baranchikov, P.V. Grachev, V.B. Loschenov, A.V. Ryabova, Comparison of concentration dependence of relative fluorescence quantum yield and brightness in first biological window of wavelengths for aqueous colloidal solutions of Nd³⁺: LaF₃ and Nd³⁺: KY₃F₁₀ nanocrystals synthesized by microwave-hydrothermal treatment, Journal of Alloys and Compounds, 756, 2018, 182–192

Osalemine rahvusvahelistel teaduskonverentsidel:

1. **E.A.Vagapova**, A.V. Popov, E.O. Orlovskaya, Z. Stankeviciute, A. Kareiva, A.E. Baranchikov, L.D. Iskhakova, I. Sildos, U. Mäeorg, S.G. Fedorenko, Yu.V. Orlovskii, Kinetics of impurity fluorescence quenching of Nd-doped hydroxyapatite Nd^{3+} : $\text{Ca}_{10}(\text{PO}_4)_6(\text{OH})_2$ powders: Nd^* -Nd self-quenching and Nd^* - OH^- quenching, 24th International conference “Optics and spectroscopy of condensed matter”, Conference proceedings, p. 308–318, September 16–22, Kuban State University, Krasnodar (2018), Eds. V.A. Isaev, A.V. Lebedev, 372 pages, ISBN 978-5-6041274-0-7
2. **E.A. Vagapova**, E.O. Orlovskaya, A.V. Popov, L. Puust, A.S. Vanetsev, Z. Stankeviciute, J. Januskevicius, M. Janulevičius, A. Kareiva, Yu.V. Orlovskii, Laser spectroscopy of bi-phasic calcium phosphate powders doped by the Nd^{3+} ions, 7th International Conference “Nanotechnologies and Nanomaterials” NANO-2019, August 27–30, Lviv, Ukraine, Book of Abstracts, p. 288
3. **Vagapova E.A.**, Studies of spectral-kinetical properties of bi-calcium phosphate micropowders, doped by Nd^{3+} ions, for biomedical applications, XVI Russian annual conference of young researchers and graduate students “Physical chemistry and technology of inorganic materials” (with international participation) proceedings of the conference, October 1–4, 2019, Moscow, Russia. IMET RAS, Moscow, Russia: IMET RAS, 179–180.
4. **Vagapova E.A.**, Janulevičius M., Strugovshchikov E., Iskhakova L.D., Vanetsev A.S., Pištšev A., Orlovskii Yu.V. Site-selective laser spectroscopy of Nd^{3+} doped beta-modification of calcium triphosphate. Functional Materials & Nanotechnologies 2020 Online Conference, Virtual Vilnius, Lithuania, 23–26 November 2020. Book of Abstract, p. 39.

Autori muud publikatsioonid:

E. Vinogradova, L. Dolgov, V.A. Konyushkin, E.O. Orlovskaya, **E.A. Vagapova**, A. Treshchalov, V. Peet, V. Hizhnyakov, Yu.V. Orlovskii, Fluorescence of Nd^{3+} optical centers close to cubic symmetry in a calcium fluoride crystal co-doped with Na^+ , Journal of Luminescence, 234 (2021) 117988.

DISSERTATIONES SCIENTIAE MATERIALIS UNIVERSITATIS TARTUENSIS

1. **Martin Järvekülg.** Tubular microstructures by Hf-, Zr- and Ti-butoxide gel sheet rolling. Tartu, 2011, 112 p.
2. **Sergei Vlassov.** Investigation of nanoscale interactions and mechanical properties of nanostructures using quartz tuning fork based real-time measurements. Tartu, 2011, 171 p.
3. **Margus Kodu.** Pulsed Laser Deposition of Magnesium Oxide and Barium Ternary Oxides for Plasma Display Protective Layers. Tartu, 2011, 89 p.
4. **Rainer Pärna.** Surface studies of some oxide films. Tartu, 2011, 129 p.
5. **Jevgeni Šulga.** Self-assembly and interaction of nanostructures. Tartu, 2011, 114 p.
6. **Wojciech Kuznik.** Quantum-chemical computer simulations of the linear and non-linear optical properties of pyrazoloquinoline and dicyanopyrazine derivatives. Tartu, 2012, 89 p.
7. **Leonid Dorogin.** Structural and tribological properties of zero- and one-dimensional nanocrystals. Tartu, 2012, 193 p.
8. **Viljar Palmre.** Fabrication and characterization of microporous carbon-based electroactive polymer actuators. Tartu, 2012, 99 p.
9. **Madis Paalo.** Synthesis of CNT-metal oxide nanocomposites: sol-gel process, rheology, structural and functional properties. Tartu, 2014, 175 p.
10. **Raul Välbe.** Development of ionic liquid composites by sol-gel method for elaboration of industrial nano- and microstructures. Tartu, 2014, 97 p.
11. **Urmas Joost.** Impurity and preparation dependent properties of titania thin films. Tartu, 2014, 155 p.
12. **Madis Umalas.** Application of sol-gel technology for production of ceramic nanocomposites and functional coatings. Tartu, 2015, 136 p.
13. **Elena Samsonova.** Energy transfer probe as a tool to study morphological and structural origins of fluorescence quenching in rare-earth doped nanophosphors. Tartu, 2015, 114 p.
14. **Jay Mondal.** Novel Corrosion Protective Nanostructured Composite Coatings. Tartu, 2016, 104 p.
15. **Kathriin Utt.** Metal oxide mesostructures for optical applications. Tartu, 2016, 88 p.
16. **Kaido Siimon.** Electrospun gelatin cross-linked by glucose. Tartu, 2016, 84 p.
17. **Marko Part.** Combined three-dimensional sol-gel structures and atomic layer deposited thin films. Tartu, 2017, 162 p.
18. **Pejman Rasti.** Analysis of Remote Sensing Image Super Resolution using Fluid Lenses. Tartu, 2017, 188 p.
19. **Ivo Romet.** Recombination luminescence of doped borates: origin and application prospects in dosimetry. Tartu, 2017, 111 p.

20. **Vladimir I. Kondratiev.** Processing and characterization of transparent electrode materials. Tartu, 2017, 111 p.
21. **Taivo Jõgiaas.** Mechanical properties of atomic layer deposited thin films and nanocomposites. Tartu, 2017, 125 p.
22. **Lauri Aarik.** Atomic layer deposition and characterization of thin oxide films for application in protective coatings. Tartu, 2017, 180 p.
23. **Triin Kangur.** Preparation and functional properties of stochastic micro-structured sol-gel silica materials. Tartu, 2018, 96 p.
24. **Marta Berholts.** Fragmentation of ionic and hydrogen-bonded molecules induced by synchrotron radiation. Tartu, 2018, 126 p.
25. **Priit Priimägi.** Development and optimization of 3D-microbatteries. Tartu, 2018, 118 p.
26. **Siim Hödemann.** Residual stress determination in chemically strengthened and thermally tempered glass plates using scattered light method. Tartu, 2019, 146 p.
27. **Jekaterina Kozlova.** Complex characterization of graphene structures on nanometer level. Tartu, 2019, 206 p.
28. **Kristjan Kalam.** Magnetic, electric and structural properties of atomic layer deposited zirconia-based nanolaminates and mixtures. Tartu, 2020, 94 p.
29. **Triinu Vihmann.** Ionic liquids: synthesis and application in lubrication and lithography. Tartu, 2020, 102 p.
30. **Helina Seemen.** Atomic layer deposition and microscopic analysis of magnetically and electrically polarizable thin solid films. Tartu, 2021, 126 p.